END

FILMED

MICROCOPY RESOLUTION TEST CHART

NATIONAL BUREAU OF STANDARDS-1963-A

AD-A163 004

ANNUAL TECHNICAL REPORT

January 1986

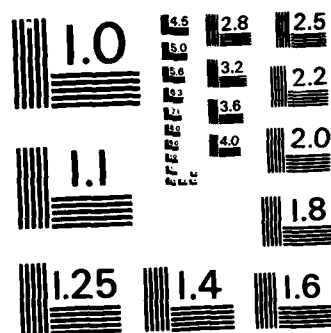OFFICE OF NAVAL RESEARCH

Contract No. N00014-84-k-0201

Whitney Award Lecture Paper

ON THE ROLES OF CORROSION PRODUCTS IN LOCAL CELL PROCESSES

H. W. Pickering

Department of Materials Science & Engineering
The Pennsylvania State University

DTIC FILE COPY

DTIC
ELECTE
JAN 0 8 1986
S   E
D

**The Pennsylvania
State University**

**University Park,
Pennsylvania**

THE PENNSYLVANIA STATE UNIVERSITY

College of Earth and Mineral Sciences

UNDERGRADUATE PROGRAMS OF STUDY

Ceramic Science and Engineering, Earth Sciences, Fuel Science, Geography, Geosciences, Metallurgy, Meteorology, Mineral Economics, Mining Engineering, Petroleum and Natural Gas Engineering, and Polymer Science.

GRADUATE PROGRAMS AND FIELDS OF RESEARCH

Ceramic Science, Fuel Science, Geochemistry and Mineralogy, Geography, Geology, Geophysics, Metallurgy, Meteorology, Mineral Economics, Mineral Processing, Mining Engineering, Petroleum and Natural Gas Engineering, and Polymer Science.

UNIVERSITY-WIDE INTERDISCIPLINARY GRADUATE PROGRAMS INVOLVING E&MS FACULTY AND STUDENTS

Earth Sciences, Ecology, Environmental Pollution Control Engineering, Mineral Engineering Management, Operations Research, Regional Planning, and Solid State Science.

ASSOCIATE DEGREE PROGRAMS

Metallurgical Engineering Technology and Mining Technology.

INTERDISCIPLINARY RESEARCH GROUPS WITHIN THE COLLEGE

Coal Research Section, Mineral Conservation Section, Ore Deposits Research Section, and Mining and Mineral Resources Research Institute.

ANALYTICAL AND STRUCTURE STUDIES

Classical chemical analysis of metals and silicate and carbonate rocks; X-ray crystallography; electron microscopy and diffraction; electron microprobe analysis; atomic absorption analysis; spectrochemical analysis.

Whitney Award Lecture - 1985

ON THE ROLES OF CORROSION PRODUCTS IN LOCAL CELL PROCESSES*

HOWARD W. PICKERING[+]

ABSTRACT

This paper reviews work performed in the author's laboratory on the roles that corrosion products play in corrosion and materials degradation processes. Subject areas include: (1) "wedging action" in which the tensile stresses required for crack propagation are generated by the formation of solid corrosion products within the crack cavity; (2) gas bubble formation and coalescence that eventually fills a major volume segment of a pit, crevice or crack; (3) an experimental determination and mathematical modeling of the local electrode potential and solution composition existing within active pits and crevices; (4) an analysis that shows the existence of a limiting electrode potential, E_{LIM}, in a cavity and defines its value; (5) an analysis based on the E_{LIM} concept and on known trends in concentrations of ionic species that provides a means for distinguishing between stress corrosion and hydrogen cracking in noble metal alloys.

REPORT DOCUMENTATION PAGE

READ INSTRUCTIONS
BEFORE COMPLETING FORM

1. REPORT NUMBER	2. GOVT ACCESSION NO.	3. RECIPIENT'S CATALOG NUMBER
Annual Technical Report	AD-A163 004	

4. TITLE *(and Subtitle)*	5. TYPE OF REPORT & PERIOD COVERED
ON THE ROLES OF CORROSION PRODUCTS IN LOCAL CELL PROCESSES	Annual Technical Report
	6. PERFORMING ORG. REPORT NUMBER

7. AUTHOR(s)	8. CONTRACT OR GRANT NUMBER(s)
H. W. Pickering	N00014-84-k-0201

9. PERFORMING ORGANIZATION NAME AND ADDRESS	10. PROGRAM ELEMENT, PROJECT, TASK AREA & WORK UNIT NUMBERS
Metallurgy Program, 209 Steidle Building The Pennsylvania State University University Park, PA 16802	

11. CONTROLLING OFFICE NAME AND ADDRESS	12. REPORT DATE
Metallurgy Branch Office of Naval Research Arlington, VA 22217	January 1986
	13. NUMBER OF PAGES

14. MONITORING AGENCY NAME & ADDRESS *(if different from Controlling Office)*	15. SECURITY CLASS. *(of this report)*
	15a. DECLASSIFICATION/DOWNGRADING SCHEDULE

16. DISTRIBUTION STATEMENT *(of this Report)*

This document has been approved
for public release and sale; its
distribution is unlimited.

17. DISTRIBUTION STATEMENT *(of the abstract entered in Block 20, if different from Report)*

18. SUPPLEMENTARY NOTES

19. KEY WORDS *(Continue on reverse side if necessary and identify by block number)*

20. ABSTRACT *(Continue on reverse side if necessary and identify by block number)*

This paper reviews work performed in the author's laboratory on the roles that
corrosion products play in corrosion and materials degradation processes.
Subject areas include (1) "wedging action" in which the tensile stresses
required for crack propagation are generated by the formation of solid cor-
rosion products within the crack cavity; (2) gas bubble formation and
coalescence that eventually fills a major volume segment of a pit, crevice
or crack; (3) an experimental determination and mathematical modeling of the

DD $_{1\ JAN\ 73}^{FORM}$ 1473   EDITION OF 1 NOV 65 IS OBSOLETE
S/N 0102-014-6601

local electrode potential and solution composition existing within active pits and crevices; (40 an analysis that shows the existence of a limiting electrode potential, E_{LIM} in a cavity and defines its value; (5) an analysis based on the E_{LIM} concept and on known trends in concentrations of ionic species that provides a means for distinguishing between stress corrosion and hydrogen cracking in noble metal alloys.

Accession For

NTIS GRA&I		
DTIC TAB		
Unannounced		
Justification		

By
Distribution/

Availability Codes

Dist	Avail and/or Special
A-1	

QUALITY
INSPECTED
3

1. INTRODUCTION

Many have contributed to the events and processes leading to my receiving the Willis Rodney Whitney Award, especially teachers, mentors, colleagues and family. I want to mention in particular, Professors Carl Wagner, Lawrence Darken, Richard Oriani, Mars G. Fontana, Frank H. Beck and Roy O. McDuffie. There are also co-authors of research papers, and some of them will be mentioned below in the text describing their work. Other co-authors worked on other topics including dealloying, stress corrosion, hydrogen absorption, surface science and electroplating. All of these studies contributed significantly to whatever progress I and my co-authors have made in furthering the understanding of the science of corrosion, the basis of the Whitney Award.

In an effort to be both historical and of interest to the broadest segment of the membership of the National Association of Corrosion Engineers, the theme indicated in the title was chosen for the Whitney award lecture. My studies on the role of corrosion products date back to graduate student days at The Ohio State University, and continue as a current research topic at The Pennsylvania State University. This paper reviews the roles that both solid and gaseous corrosion products play in local cell processes. Some results from other laboratories will be mentioned but no effort will be made to review the literature. Although the various studies described were done with a view towards improving our understanding of localized corrosion, the results impact on other areas of corrosion and corrosion protection, including stress corrosion, hydrogen cracking, cathodic protection, inhibitor effectiveness and coating delamination.

This paper has several sections and subsections as follows:

2. WEDGING ACTION BY SOLID CORROSION PRODUCTS

At The Ohio State University in the early sixties, there was great interest in knowing what role, if any, solid corrosion products played in promoting stress corrosion cracking (SCC). Nielsen (1) had recently presented a paper which, more convincingly than any previously, showed that stress corrosion cracks in stainless steel were full of solid corrosion products. This observation added credence to the hypothesis that solid corrosion products, if larger in volume than the metal from which they form, would exert a "wedging action" when forming under constrain. Shortly thereafter, Pickering, Beck and Fontana (2) published a paper, described below, that clearly showed (a) the existence of a wedging effect, and (b) that stress corrosion cracks can be

initiated and propagated by the formation of solid corrosion products in a cavity or crack. Prior to this time, there were no recognized wedging-action failures in industry. In more recent times some of the more spectacular wedging-action failures include the "denting" problem in nuclear reactors, and the disintegration of bridge decks and pavement due to the upheval of concrete around corroding steel reinforcing bars.

2a. Stainless Steel

M. G. Fontana, then Professor and Chairman of the Department of Metallurgical Engineering, The Ohio State University, had a great interest in knowing whether or not a wedging effect could occur inside cavities and, if so, would be sufficient to cause SCC at the base of the cavity. This question set the boundaries for my Ph.D. thesis, a research effort which answered both parts of the question in the affirmative for austenitic stainless steel. It also yielded semi-quantitative information on the pressures developed on the crack walls by the expanding corrosion product, and on the tensile stresses transmitted to the crack tip. And, it unequivocally showed that a wedging effect in notches could initiate a stress corrosion crack, and that, once initiated, could propagate due to further wedging action within the crack.

The SCC of stainless steel had been successfully studied for years at the OSU corrosion laboratory, so some of the procedures for the wedging action studies were already established. These included the use of an autoclave heated to 204°C for austenitic stainless steel in an aqueous chloride-containing solution. However, instead of supplying a load with a C-clamp or other loading device, the sample, Type 304L or 347 stainless steel, was placed in the autoclave free of any residual or applied loads. To avoid residual stresses, the sample was furnace cooled following the stress relief anneal, acid treated and inserted in the autoclave above the solution. During the test the vapor

over the solution condensed on the autoclave top and dripped on the sample. In addition, the solution was made more acid than usual to increase general corrosion and, consequently, also the rate at which solid corrosion products formed. Compositions of the stainless steels and solutions are listed in Table 1.

Notches were milled in the samples. After stress relieving, most but not all of the volume of the notch was purposely filled by inserting a loosely fitting plate of the same stainless steel. During the autoclave test, solid corrosion products formed and filled the remaining gap between the plate and walls of the notch. This experiment illustrated the initiation and propagation of cracks at the base of the notch, as a result of wedging by solid corrosion products along the walls of the notch, as shown in Figure 1. The cracks propagated transgranularly, a characteristic of SCC in austenitic stainless steel in chloride solutions.

The above test illustrated the initiation and propagation of stress corrosion cracks as a result of wedging action in a notch, but did not answer the question about wedging action due to solid corrosion product formation within the crack itself. This question was answered in another experiment. Again, stress relieved samples were used. These contained stress corrosion cracks from a previous experiment. It was found for these samples that some of the cracks propagated as a result of solid corrosion product formation within the preexisting cracks. These samples were under zero applied load. In one experiment the plate was removed from the notch (refer to Figure 1) after cracking has been initiated at the base of the notch. Then, during further autoclave testing, some cracks propagated over several of their original lengths. In another test, a stress corrosion crack was introduced in a smooth surface by slightly deforming (elastically) the sample in bending while in the autoclave, and then the bending load was removed. The largest tensile stress

(at the outer surface) due to bending was only approximately 2000 psi, too small to introduce significant residual stresses. In subsequent autoclave tests, propagation of preexisting cracks occurred, as illustrated in Figure 2.

Pressures developed by corrosion product formation for the stainless steels and solutions in Table 1 were determined by measurement of the expansion of a thin walled, essentially inert, titanium cyclinder of approximately 1.3 cm diameter. Its expansion was caused by corrosion products that formed between the corroding stainless steel sample placed concentrically inside the cyclinder and the inside wall of the cyclinder. This arrangement is shown in the insert of Figure 3. Expansion of the Ti cyclinder as a function of time in the autoclave at 204°C is also shown in Figure 3. Corrosion product pressures of 4000 to 7000 psi were calculated from these data. These pressures corresponded to estimated tensile stresses at the base of the notch in the vicinicy of the yield stress. Details of these and other experiments can be found elsewhere (2).

Table 1. Compositions of the Stainless Steels and Aqueous Solutions
Used in the Wedging Experiments (2).

Stainless Steels	C	Ni	Cr	Si	Mn	P	S	Cb
Type 347	0.07	10.36	17.15	0.61	1.48	0.018	0.015	0.97
Type 304L	0.029	8.84	18.24	0.38	1.42	0.033	0.010	

Solutions

2% NaCl - 3% HNO_3

42% $MgCl_2$ - 3% HNO_3

2b. Steel Reinforced Concrete

The deterioration of steel reinforced concrete used on bridges and roadways is a well recognized national problem. It has been attributed in some instances to the corrosion of the steel reinforcing bars, formation of solid corrosion products, and wedging action that causes cracking and spalling of the concrete.

Although little information exists to support this theory, some experimental confirmation was provided in a relatively recent study by K. Rosengarth and J. H. Hoke in our corrosion laboratory at The Pennsylvania State University (3).

A procedure for measurement of the magnitude of the stresses developed during corrosion of the steel reinforcing bars (0.33% C, normalized, primary ferrite and pearlite) in laboratory specimens was developed, patterned on the design in Figure 3. The specimen consisted of four basic components: the steel center, a ring of mortar concentric around the steel, an outer ring of titanium around the mortar and electrical resistance strain gages attached to the outer surface of the titanium. This design and the measured expansion of the Ti cyclinder due to wedging action are shown in Figure 4. The specimen was partially immersed in an aqueous NaCl solution at room temperature, either at open circuit or under anodic polarization. The measured wedging action is the result of corrosion of the steel reinforcing bar with the formation of solid corrosion products in the space between the steel and mortar. Stresses exerted on the annular mortar were transmitted in large part to the titanium ring and registered on the strain gages. The wedging action could be accelerated by increasing the rate of corrosion product formation using applied anodic polarization. In some experiments, galvanized steel was used, in which case zinc corrosion products were mainly formed. Some wedging action occurred with the galvanized steel, although less than for the bare steel.

3. GAS ACCUMULATION WITHIN CAVITIES

In addition to providing a wedging action, solid corrosion products decrease charge and mass transfer between the crack tip and the outer surface of the sample. Although little information is available, it is known that both the electrode potential and solution composition, within a local cell, differ from their respective values at the outer surface. Gaseous corrosion products can

also accumulate in pits, crevices and cracks, and are known to disrupt charge
and mass transfer. The data supporting these statements are presented below.

The effects of gas accumulation in cavities have been studied in our
corrosion laboratory, starting in the early seventies at the then Edgar C. Bain
Laboratory for Fundamental Research of the United States Steel Corporation, and
continuing to the present time at The Pennsylvania State University. These
studies have produced a somewhat different type of experimental data and a
nonconventional understanding of the mechanism of localized corrosion. The
traditional view relies on composition differences between the cavity solution
and outer bulk solution, as the basis for explaining a stable localized
corrosion event. Implied in the use of this premise is the assumption that
differences in electrode potential between the cavity and outer surface are
either nonexistent or insignificant. On the other hand, if one develops an
understanding based on a lower overpotential inside the cavity, a picture
emerges in which the electrode potential within the local cell is the key
parameter. The importance of compositional differences in stabilizing local
cell action is less so, i.e., changes in solution composition could be merely a
consequence, through with some significant ramifications, rather than a cause,
of the local cell process. The experimental findings are (1) that potential
differences generally exist during localized corrosion, for either open circuit
or anodic polarization conditions, as well as during cathodic polarization, and
that in an active local cell they can be surprisingly large. The simultaneous
observation of a strong tendency for H_2 gas to accumulate and exist as stable
bubbles inside pits and crevices in ferrous alloys, Ni and Cu has been
hypothesized to be an important related event, often stabilizing large potential
differences, during open circuit, anodic or cathodic polarization conditions.

In the past, in the absence of information, the often invoked assumption of a nearly constant potential was usually justified on the basis of the good conductivity of most aqueous electrolytes, and on the additional implicit assumption that gaseous and solid corrosion products do not significantly decrease charge and mass transfer. A close look at the literature produces only an occasional mention of measured potential differences prior to the early seventies (4-6). Furthermore, virtually no information was available on the second assumption. Pits and crevices were known to often contain solid corrosion products. Although there were a few reports of gas evolution from pits (7-9), no mention was made of gas accumulation within the pits. The observation of gas evolution could have provided insight on the magnitude of the electrode potential inside the pits, had the gas been identified as hydrogen, and had the potential at the outer surface of the sample been measured and found to be noble of that needed for hydrogen evolution to occur (at the outer surface). Then, it would have been clear, in those early studies of localized corrosion, that a significant potential difference existed between the inside and outside of the pit. Notice that the observation of H_2 gas coming out of pits has no special significance if the potential at the outer surface is in the range of hydrogen evolution, as would normally be the case for pitting of aluminum and other highly reactive metals under open circuit conditions. This kind of analysis has since been made, and is included below in a review of the extent of gas accumulation in, and evolution from, pits and crevices; and on the effect of accumulated, "in-place" gas, on the value of the electrode potential in the cavity, especially with regard to its location on the operative polarization curves.

3a. Anodic Polarization and Open Circuit Conditions

Some of the early experiments on localized corrosion, performed with R. P. Frankenthal, revealed the existence of gas accumulation in pits in iron and stainless steels (10,11). Using a stereomicroscope (and a movie camera) positioned over the cell, as shown in Figure 5, gas bubbles were clearly observed rising out of naturally occurring pits in iron samples and recorded on film during the pitting process, as shown in Figure 6. These samples were anodically polarized over a wide range of potential in a NaCl containing sulfuric acid solution. A more complete description of the experimental arrangement is given in Section 4. Each cluster of white specks (light reflections off the faceted internal surfaces of the pit) in Figure 6 is a single pit. In (b) a bubble is just emerging from the (outlined) pit. In (c) and (d) the bubble is rising within the electrolyte and is easily recognized by the two, large diffuse spots, one of which is a reflection. For the higher pH solutions (within the range, pH 0-6), the rising bubbles contained fragments of solid corrosion product. This observation of attached fragments was confirmed when residue was left on the surface of the solution as the gas bubble entered the air over the solution. Bubbles also rose from pits along grain boundaries

Closer in-situ examination of the insides of pits with the microscope revealed that they contained accumulated gas for every system studied, including also stainless steels and other electrolytes, and for both anodic polarization and open-circuit (corrosion) conditions. For the low pH solutions, for which visibility within the pit was not obscured by solid corrosion products, the accumulated gas was observed to be in a state of motion. For the other systems, the bubbles were observed when the contents of the pit or crevice were disturbed with a glass fiber.

The gas rising out of pits in an iron sample polarized to 1 V (SHE) was collected and found by mass spectrometry to be hydrogen. The O_2 content of the collected gas was low, indicating that oxygen was reduced at the specimen surface during the corrosion experiment. The formation of hydrogen inside the pit of a sample whose outer surface is over 1 volt positive of the hydrogen evolution potential, clearly shows the existence of a much lower ($\lesssim$ 0.0 volts, SHE) electrode potential within the pit.

3b. Cathodic Polarization Conditions

In another set of experiments with B. Ateya and graduate students D. Harris and A. Valdes, gas bubble accumulation within crevices was observed for cathodic polarization conditions. In the first of these experiments (12), crack-like slots of cross section, 0.5-1.5 mm by 1.2 cm, and depth 1.2 cm, were cut in the middle of cubes of Ferrovac E Fe, electrolytic Ni and 99.999 Cu, and tight-fitted into a Teflon mount such that only the outer top and inner slot surfaces were accessible to the electrolyte. The sample was put into a large volume of either 1M $HClO_4$ or 0.5 M sodium acetate-0.5 M acetic acid (pH = 5) at room temperature. A constant cathodic current of 50 or 100 A m^{-2} was impressed on the samples, sufficient to provide full cathodic protection of the outer surfaces of all three metals. Thus, hydrogen evolution is the only reaction maintaining the impressed current.[+]

For all three metals, gas accumulation and the existence of stable in-place gas were observed within the slots. The relatively large width of the slot in

[+]except to the extent that other reactions, specifically metal dissolution, can occur within the slots due to shifts in the local electrode potential and solution composition from the outer surface values; this phenomena is discussed in Section 4.

the nickel sample enabled additional information to be obtained on the nature of gas bubble formation and evolution within the slot. It was seen that accumulation of the gas occurred to give a large bubble which occupied most, if not all, of the cross section. Intermittently, smaller H_2 bubbles, though much larger in size than those evolving off the outer top surface, evolved from the slot. In most cases the observed evolving bubbles were breakaway gas from the large in-place bubble.

In order to facilitate viewing the gas accumulation process, an Fe sample was modified so that one side of the slot was made of a transparent plastic (13). The H_2 gas which formed by the hydrogen evolution reaction (h.e.r.) and readily evolved off the sample's outer and slot surfaces, also accumulated within the previously gas-free slot into the large in-place bubbles seen in Figure 7. The slot in Figure 7 was relatively large (0.5mm x 5mm x 9mm) in terms of real crevices and very large in terms of most cracks. However, in spite of its size, the (large, in-place) H_2 bubbles readily formed in the slot and filled its cross section. Since gas bubble accumulation occurred for both crevice designs, it was clear that the formation and stability of the in-place H_2 bubbles within the crevices were characteristic of metal crevices and not of the plastic surface used for better visual observation in the modified design.

The nature of the solution affected the tendency for H_2 gas accumulation. In preliminary tests, accumulation occurred more readily in the acetate, than in the perchloric acid, solutions (15). The former was used to obtain the above results. Preliminary tests to evaluate various surfactants showed that additions of sodium dodecyl sulfate to the acetate solution inhibited the clustering of smaller bubbles into larger ones (15). As a result, the tendency for gas accumulation inside the cavity, in the presence of this compound, was reduced.

3c. A Test of the Traditional View of Localized Corrosion.

In another experiment an interesting result was obtained that was inconsistent with the traditional view of localized corrosion. Using the same basic sample design as in Figure 7, the stability of hydrogen gas within the slot, was tested under anodic polarization conditions (15). The hydrogen bubble was found to be quite stable when the polarization on the sample was switched from cathodic to anodic, i.e., the H_2 bubble maintained its size and position in spite of the fact that at the outer surface approximately one volt overpotential existed for the oxidation of the hydrogen to its H^+ ions. Furthermore, the bubble showed less motion and more apparent adherence to the slot walls, than for the cathodic polarization condition under which it formed. A day or more could pass without any marked change in its position or size. The question to be answered is: How could such stability exist at one volt over potential for the oxidation of the gas? The traditional view of localized corrosion, that has a change in composition as its basis, has no answer to this question, whereas the potential shift theory does, as follows.

There appears to be two plausible explanations of the stability of the H_2 bubble during anodic polarization to potentials well above the stability range of H_2 gas. The first is slow kinetics of the hydrogen oxidation reaction, which can not be disregarded even considering the magnitude of the overvoltage and the time of that test. The second incorporates information to be described in Section 4 on the largely different electrode potentials at the outer region of the bubble near the slot opening, and at the inner region inside the slot. The measured potentials in these two locations are typically very different, with that inside the slot being the less noble, as described in Section 4. Thus, it is conceivable that hydrogen discharge occurs within the slot where the local electrode potential could be less than E_{H/H^+}, i.e., by the reaction,

$$H_3O^+ + e^- \rightarrow 1/2H_2 + H_2O \tag{1}$$

while, at the same time, oxidation of hydrogen occurs at the opening of the slot where the local electrode potential is approximately equal to that established at the outer surface with the potentiostat. The latter electrode potential corresponds to a high overpotential for oxidation of hydrogen gas by Reaction (1) proceeding to the left, instead of to the right. Thus, the size and position of the bubble would change until these two reactions occur at the same rate. Thereafter, the bubble size and position would be stablized by this dynamic equality of two opposing reaction processes.

3d. <u>Initiation of Localized Corrosion at the Bubble/Metal Interface</u>

During the long periods of stability of the bubble under anodic polarization conditions described in 3c, a new localized corrosion event, a pit or crevice, often occurred at the bubble/iron interface, and penetrated into the iron normal to the slot wall (15). An advanced stage is illustrated in Figure 8. This heavily corroded wall of the crevice was originally smooth. The corrosive attack only occurred where the bubble contacted the wall (near the top of the slot in Figure 8).

4. ELECTRODE POTENTIAL INSIDE CAVITIES

The observation of gas accumulation inside cavities described in Section 3 for a wide range of electrode potential existing at the outer surface, including anodic and cathodic polarization, was accompanied by simultaneous direct measurement of the local electrode potential and of the solution composition inside the cavity (10-15). The experimental arrangement mentioned in Section 3a and illustrated in Figure 5 is more fully described here. The cell was an open beaker that contained the iron sample and platinum wire counter electrode. A Luggin capillary, positioned close to the specimen surface, connected the main

cell compartment to a second compartment containing a saturated calomel reference electrode. The three electrodes were connected to a potentiostat in the usual manner.

For the measurement of electrode potential inside a local cell, an additional microprobe reference electrode was used. It consisted of a glass capillary drawn to a fine tip, ~0.005 cm in outside diameter, and connected to a glass vessel containing a Hg/Hg_2SO_4 reference electrode by a salt bridge containing the same electrolyte solution as in the main cell. Visual examination and measurement of the resistance of the microprobe assembly were used to determine when it was completely filled with the solution. The microprobe is attached to a 3-directional micro manipulator with a resolution of 2.5 µm in each direction (Figure 5). The microprobe measures the electrode potential across the metal-solution interface plus any potential drops that exist between the solution side of the interface and the probe tip.

Electrode potential values obtained inside the pit by this procedure are reliable, based on the following observations (10-14):

[1] With the sample surface anodically polarized to 1.0 V (SHE) in air saturated 0.5M H_2SO_4+3mM NaCl (pH 0.3), the gas forming within, and escaping from growing pits in iron, was analyzed to be H_2 (Section 3a). This places the local electrode potential in the pit at a value of ⪡ 0.0 V (SHE). The actual value was dependent on the local h.e.r. current and pH. The measured value was more noble than the actual value by the magnitude of the IR between the probe tip and the site of the most negative electrode potential in the local cell. The measured values were typically in the range, -0.2 to 0.2 V (SHE), and are reported in detail below.

[2] In iron samples anodically polarized to 0.7 to 1.2 V (SHE) at the outer surface and also in stainless steel samples anodically polarized to 1.0 V (SHE),

the walls of the pits prior to salt film formation were observed to be faceted, as shown in Figure 6. This faceting was due to the differences in crystallographic orientation, and is typical of dissolution in the active region, in particular in the Tafel region. This would place the local electrode potential of the faceted surface at less.than approximately -0.2 V (SHE) (10), which is also in good agreement with the measured values given in [1].

[3] In iron and nickel samples cathodically polarized to -0.9 and -0.7 V (SHE) at the outer surface, respectively, metallic ions of the sample were found to have formed inside of the slots (12). Since Fe and Ni dissolution are inconsistent with these potentials, that correspond to a state of complete cathodic protection, it follows that the electrode potential inside the slot was more noble than these outer surface values. Furthermore, the magnitude of the shift in potential must have been considerable based on the standard potentials of -0.44 and -0.25 V (SHE) for iron and nickel, respectively. This reasoning (12) is consistent with the most oxidizing measured values in the slot of approximately -0.2 V, SHE. In copper samples cathodically polarized to -0.7 V (SHE), at the outer surface, copper ions would not be expected to form and didn't. This is because the standard potential of copper is more noble by over 300 mV than the equilibrium potential of the h.e.r., the latter being E_{LIM} for the system as described in Section 4d. Therefore, the measured electrode potential in the slot of approximately -0.2 V (SHE), reported below, is less than E^{eq}_{H/H^+}, as it must be and, therefore, also lower than $E^{eq}_{Cu/Cu^{++}}$.

The measured electrode potential in the cavity is generally recognized to only approach E_{LIM}. This largest ohmic voltage required to produce an electrode potential close to E_{LIM} is expected to occur in the most constricted regions, e.g., between the bubble and cavity wall and, therefore, not be measurable because the conditions producing it are affected by the probe itself.

4a. **In the Presence of Gas Accumulation**

During the gas accumulation processes described in Section 3, the local electrode potential and, to some extent, solution composition, were monitored in an effort to more fully characterize the important parameters in local cell processes. In particular, our focus has been on the effect of gaseous corrosion products on the electrode potentials existing inside of the cavities, for constant electrochemical conditions at the outer surface. Such data are needed for a better understanding of the mechanisms of local cell processes, such as localized corrosion and the failure of cathodic protection systems.

Using the potential probe described above, the local electrode potential was measured as a function of distance into gas-filled cavities, and as a function of the extent of occupancy of the cross section of the cavity by the gas. For well operating probes, some inconsistency was, nevertheless noted, and was believed to be due to the lack, in particular in those cavities that were not gas filled, of an active local cell in the cavity. The best indication of the presence of an on going local cell is an increase in cavity size, in the case of anodic polarization including open circuit conditions; and the presence of gas, along with its accumulation and/or evolution, for both cathodic and anodic polarization conditions. In the absence of an ongoing local cell, the measured local electrode potential within the cavity does not differ significantly from that at the outer surface of the sample.

There are three possibilities for a local cell electrode potential to be close in value to the electrode potential at the outer surface: (1) the local cell is inactive, (2) the electrode potential at the outer surface, established either by externally applied polarization or open circuit conditions, is close in value to the limiting electrode potential described below in Section 4d, and/or (3) the local cell is active but the cross section of the cavity is

relatively open to the bulk solution, thereby providing for easy mass and charge transfer in and out of the cavity. The situation in (3), however, probably can not actually exist, i.e., a fully open or nonconstricted cavity may not support an on going local cell. Constrictions that limit mass and charge transfer consist of corrosion products, either solid or gaseous, filling the cavity, and/or a remaining film of passivated metal at the sample's surface that covers most of the cavity's cross section. Both types of constrictions are regularly observed in localized corrosion. An often important consequence of the constriction is a large ohmic potential drop between the local cell in the cavity and the outer bulk solution, as mentioned above and described below.

Large ohmic potential variations within the electrolyte connecting the local cell and bulk solutions appear to be characteristic of localized corrosion and of certain failure modes during cathodic protection. Although, occasional reports of large potential variations between the local cell and bulk solution appear in the early literature, they were not usually associated with the electrode potential at the site of the local cell, being instead overlooked or rationalized in other ways, e.g., as a potential drop across salt films and, in general, missing the mark of their actual physical significance. The particular measurement method described above is capable of measuring only changes in electrode potential between the local cell and bulk solutions. Any potential drops existing across films on the sample, either in the slot or on the outer surface, would go undetected and be additional voltage changes to those measured.

i. **Anodic Polarization.** What we have consistently observed for iron systems with the potential at the outer surface in the passive region, is that during pitting or crevice corrosion, the electrode potential at the site of the (active) local cell is much less noble and often approaches the limiting

electrode potential, E_{LIM}, of the system. This is illustrated schematically in Figure 9. In essence, Figure 9 shows that the electrode potential inside an on going pitting or crevicing situation is at a value relatively close to the reversible potential for metal dissolution (E_{LIM}), for which the system tends to be active rather than passive. Although, oscillatory behavior normally is not observed, it can be induced by the probe, and is also schematically illustrated in Figure 9. The amplitude of these potential variations with time can be so large that the local cell oscillates in an irregular fashion between active and less active or passive behavior. This experiment provided an important insight into the pit growth mechanism when the current flowing out of the cavity was simultaneously measured, as shown in Figure 10. The spikes in potential variation within the electrolyte, with the probe at two different positions inside the pit, are matched exactly by spikes in the pitting current. This was, and may still be, the only direct evidence of a correspondence between the electrode potential at the site of an active local cell within the pit and the pitting current. There is no comparable evidence of such a relationship between the solution composition in the local cell and the pitting current, whereas, the traditional view of localized corrosion would predict one since its foundation is an enrichment of the local cell solution in aggressive anions and/or H^+ ions.

Data of the type in Figure 10, therefore, are another reason to suggest that compositional variations perhaps should be viewed more as a consequence, rather than a cause, of localized corrosion. Yet, there are well established effects of composition on the pit growth process. The effect of chloride ion is usually attributed to its degrading of the passive state. In addition, the chloride ion concentration increases in the local cell solution with increasing ϕ potential (or with the equivalent more negative electrode potential described

below in Eq (2) at the site of the local cell), as shown elsewhere (10). In

terms of the oscillatory potential behavior in Figure 10, this Cl^- ion effect

translates into expected higher currents during swings of the potential both

into the active and passive regions (refer to Figure 11d).

The effect of acidification in promoting the pitting process could have a

similar explanation, in that the passive potential region contracts or,

conversely, the active region expands, with increasing acidification (refer to

Figure 11e). Acidification occurs in the local cell due to hydrolysis reactions

when the bulk solution is at a pH that is above that for equilibrium of the

hydrolysis reaction, e.g., acidification typically occurs for a pH 7, but not

for a pH 0, bulk solution. In the absence of hydrolysis, e.g., for the pH 0

bulk solution, the pH of the local cell solution actually increases, rather than

decreases, to the pH of the hydrolysis reaction due to the potential ϕ (10).

Compositional effects also could enter in more subtle ways, such as through

their effects on gas bubble formation and/or stability within the cavity.

These changes in local electrochemistry inside active pits or crevices are

summarized in Figure 11. The scheme in (a) illustrates the large shift in

electrode potential with distance into the cavity, described above for active

pits or crevices. In (b) and (c), the traditional views of pit and crevice

growth are illustrated. Combined effects of potential and composition are shown

in (d) and (e).

Most known cases of localized corrosion could be explained by any one of

the five possibilities illustrated in Figure 11. Therefore, a determination of

the potential and solution composition within the local cell would be needed to

single out the actual mechanism. There are situations, however, that can only

be explained by one or two of the schemes in Figure 11. Crevice corrosion in a

low pH solution, free of aggressive anions such as chloride, would seemingly

only be possible by the scheme in (a).

There is also a sometimes-observed morphology of localized corrosion (10, 11) that has never been satisfactorily explained by either scheme (b) or (c), but appears to have a reasonable explanation in the potential shift concept of schemes (a), (d) or (e). In crevice corrosion of stainless steels, the corrosion process occurs underneath the surface into the bulk of the steel from the crevice wall. Soon, a penetration of the surface of the stainless steel occurs from underneath. However, once the penetration occurs, active metal dissolution at the site of the penetration ceases, or slows considerably below that occurring elsewhere in the crevice. As a result, other penetrations, that also lead to a sharp decrease of the corrosive action at the penetration, occur elsewhere on the surface. Eventually, a highly perferated metal surface layer covers the crevice volume.

A similar phenomena has been reported for localized corrosion occurring at inclusions in stainless steels, in which case a corrosion front moves underneath the surface radially outward from the inclusion. As in the above case of crevice corrosion, penetrations of the surface from underneath soon appear. They are in a somewhat arranged pattern concentric with the inclusion. This produces a pattern of penetration sites that has been referred to as lace-like in the literature (10, 11). Another example of a lace-like pattern has been observed at corroded grain boundaries in sensitized Fe-20Cr ferritic stainless steel (16).

One explanation of this "perforation" phenomena is that when penetration occurs the potential difference ϕ between the local corrosion site and the bulk solution, that was maintaining the local cell electrode potential in the active region, vanishes and the electrode potential at the penetration site jumps to a more noble value approaching the outer surface value for which passivity is

maintained. Thus, referring to Figure 11, scheme (a) is sufficient in itself to explain this phenomena. Schemes (d) and (e) could also be operative to the extent that mixing occurs between the local cell electrolyte and the bulk solution when the penetration occurs. Convective mixing would probably not be significant, so the extent of mixing would depend on the relatively slow diffusive transport process.

The operative local cell inside a crevice can also occur nearer to the mouth of a narrow crevice, compared to a more open crevice, as illustrated in Figure 12. This has been observed by Miyuki and coworkers (17) for Type 304 stainless steel in artificial seawater. Although the detailed conditions that produced this result need to be established, the phenomena appears to be consistent with some results of a theoretical study by Ateya and Pickering (12). In this paper it was found that as a crevice narrows, the electrode potential gradient within the crevice steepens. This means that as one moves into a crevice, the active/passive boundary, $E_{A/P}$, is encountered sooner (nearer the crevice mouth), the narrower is the crevice. Thus, $E_{A/P}$ is one of the boundaries of the local cell corrosive action in the crevice, and the other boundary, further from the crevice mouth, is the E_{LIM} potential, as illustrated in Figure 12. The modeling in Reference 12 was done for the h.e.r. reaction in a crevice-like slot and is presented below in Section 4b.

ii. <u>Cathodic Polarization.</u> Clearly, if accumulated gas can cause large changes in the local electrode potential at the site of a local cell during anodic polarization, why not also during cathodic polarization for which H_2 gas accumulation also occurs, as illustrated in Figure 7? Using the potential microprobe described above, large changes in electrode potential, accompanied by accumulating gas, have been observed within crevice-like cavities during cathodic polarization of Fe, Ni or Cu samples in acids of pH 0 to 5 (12-15).

Values are given in Table 2. In the experiments ϕ_x was measured, and E_x was obtained for preset values at the outer surface, $E_{x=0}$, from the relation (18)

$$E_x = E_{x=0} - \phi_x \tag{2}$$

Eq. (2) shows that $E(x)$ shifts in the less noble direction for an oxidation reaction occurring within the cavity (ϕ_x is (+) for current flowing out of the cavity), and in the more noble direction for a reduction reaction (ϕ_x is (-) for current flowing into the cavity), corresponding to a reduced overpotential for both reactions with increasing x. An increase in E_x to more positive values with increasing distance x into a cavity during cathodic polarization is schematically illustrated in polarization plots presented in Section 4d in a discussion of E_{LIM}, including Figure 18b for the noble metal copper in the $HClO_4$ solution for which $E^{eq}_{Cu/Cu^{++}}$ is more noble than E^{eq}_{H/H^+}, and Figure 19b for the Fe and Ni samples in their respective solutions given in Table 2. For anodic polarization, E_x decreases with increasing x, as shown in Figures 11, 18a and 19a.

Table 2. The measured potential drop in the crevice solution, ϕ, and electrode potentials $E(x=0)$ and $E(x=L)$ (SHE), where x = 0 is at the crevice mouth and x = L is at its bottom (12).

Metal	Solution	i_s,A m^{-2}	$E_{x=0}$,V	$\phi_{x=L}$,V	$E_{x=L}$,V	Estimated E_{LIM},V
Fe	0.5M NaAc 0.5M HAc (pH=5)	50	-0.9	-0.4	-0.5	E_{mixed} = -0.4
Ni	1M HClO$_4$	100	-0.7	-0.5	-0.2	E_{mixed} = -0.1
Cu	1M HClO$_4$	100	-0.7	-0.5	-0.2	E_{equil} = 0.0

As the in-place H_2 bubbles formed, the measured potential gradients within the crevices were found to increase markedly to the values in Table 2. Thus, gas accumulation within the slot was responsible for the large magnitude of the potential shift. The measured solution potential for the Fe sample, expressed in terms of $\phi_{x=0} = 0$, where x=0 is at the crevice mouth (Figure 13), is given in Figure 14, with and without in-place H_2 bubbles in the cavity. The upper curve corresponds to in-place H_2 bubbles of size comparable to the crevice cross section, as shown in Figure 7.

In the region of contact of the H_2 bubbles with the iron (Figure 7) and at greater distances into the cavity, the iron underwent anodic dissolution as revealed by the etched condition of the crevice wall (originally polished) in Figure 15. This etching occurred during effective cathodic protection of the sample's outer surface in accord with the large ϕ value caused by the accumulated gas. The polarization plot in Figure 19b corresponds to this situation, in which E_x shifts from the surface value, $E_{x=0}$, into the region of metal dissolution.

Other experiments were performed on Fe, Ni or Cu samples to test for anodic dissolution within the crevices. In these experiments solution was extracted from the crevice during cathodic protection of the outer surface, and analyzed for metal ions. The results of these analyses are shown in Table 3. The true metal ion concentrations in the crevices were much larger than the measured values given in Table 3 because of a large dilution of the crevice solution during extraction. In contrast to the dissolution of Fe and Ni within their crevices, the solution in the Cu crevice contained no copper ions within the accuracy of the measurement, in accord with the E_{LIM} condition as explained below. Qualitative tests for iron were done using the Standard

Orthophenathroline color procedure. Quantitative tests for Fe, Cu or Ni ions
for the different metal samples were made by atomic absorption spectrometry
(flame) using blank and standard solutions consisting of the bulk electrolyte
and known concentrations of the metal ion.

Table 3. The measured concentrations of M^{2+} in electrolyte extracted from
crevices or bulk solution for conditions in Table 2 (12).

Metal	Bulk$[M^{2+}]$ (ppm)	"Crevice"$[M^{2+}]$ (ppm)
Fe	2	50
Ni	0.2	15
Cu	---	1

4b. Effect of Cavity Dimensions

Mathematical modeling of the h.e.r. in crevices has been successful in the
case of crevices free of gas (dashed curve in Figure 14). An important feature
of these models is that they allow the reaction to occur on the crevice walls
and treat the reaction rate as an unknown in the calculation (12). This has not
been done in the corresponding mathematical modeling for anodic polarization
conditions (10). Introduction of this feature in the model brings into play the
effect of the dimensions of the cavity on the potential and ionic
concentrations. The calculation which follows for a crevice geometry shows that
the width of the crevice is a very important parameter.

Let us consider the h.e.r. in a simple strong acid HY of monovalent ions
and a crevice geometry shown in Figure 13. The cross section of the crevice is
a rectangle of dimension $\underline{a}$ and $\underline{b}$, and its depth is L such that $\underline{a} \ll L$ and $\underline{a} \ll$
$\underline{b}$, in which case the h.e.r. can be considered to occur only on the outer
surface and on the crevice or crack walls. A more precise condition for
validity of the equations is $X \gg \underline{a}$ where X is a characteristic distance defined
below. Implicit in the calculation is the assumptions that ionic interaction is

not significant. This assumption is reasonable for the purposes of the calculation and, in any case, is increasingly more valid with increasing distance into the cavity since the total ionic concentration decreases. It is also assumed that gaseous reaction products do not accumulate inside the cavity. This assumption is often inappropriate as shown above. When gas or solid constrictions are included in the model, larger ohmic and ionic gradients are calculated. The flux equations and the model also assume negligible convective transport within the cavity. As such the model most closely describes the transport processes in quiescent, gas-free cavities during the h.e.r.

The fluxes, j, of the H^+ and Y^- ions in the x direction within the crevice/crack are

$$j_{H+} = -D_{H+} \left(\frac{dc_{H+}}{dx} + c_{H+} \frac{F}{RT} \frac{d\phi}{dx} \right) = \frac{i}{F} \tag{3}$$

$$j_{Y-} = -D_{Y-} \left(\frac{dc_{Y-}}{dx} - c_{Y-} \frac{F}{RT} \frac{d\phi}{dx} \right) = 0 \tag{4}$$

where D and c are the diffusivity and concentration of the indicated species, respectively, ϕ is the solution potential with respect to $\phi = 0$ at $x = 0$, and i is the current density as a function of x on the crack walls for the impressed h.e.r. current on the sample surface, i_s. The electroneutrality equation is

$$c_{H^+} = c_{Y-} = c \tag{5}$$

The boundary condition at x=0 for a bulk acid concentration of c_o is

$$c_{H+} = c_{Y-} = c_o \text{ and } \phi = 0 \text{ at } x=0 \tag{6}$$

A boundary condition at $x = L$ evolves from the calculation which can be found elsewhere (12). Equations (3) to (6) are then used to obtain ϕ, c_{H+}, c_{y-} and i as functions of x, c_o, $\underline{a}$ and i_s.

The characteristic length X is obtained as (12)

$$X = (D_{H+} \, c_o \, F \, \underline{a}/i_s)^{1/2} \tag{7}$$

and the solutions for the unknowns are (12)

$$\phi = \frac{RT}{F} \ln \frac{\cosh [(L-x)/X]}{\cosh [L/X]} \tag{8}$$

$$c_{H+} = c_{Y-} = c_o \frac{\cosh [(L-x)/X]}{\cosh [L/X]} \tag{9}$$

$$i = i_s \frac{\cosh [(L-x)/X]}{\cosh [L/X]} \tag{10}$$

In addition, ϕ is related to the local electrode potential, E_x, in the cavity by Equation (2). Equations (8) and (2) may be used to estimate the distance into the crevice at which the electrode potential assumes a sufficiently noble value for anodic dissolution of the metal, within the constrain of E_{LIM}. Equation (9) and (10) may be used to estimate the distance at which depletion of H^+ and decrease in the hydrogen evolution rate become significant. Equation (8) is the dashed curve in Figure 14 and compares well with the measured curve (lower solid curve) for experimental conditions which, although not exactly matching the model conditions, are for a bubble-free crevice.

An important feature of Equation (8) using also Equation (7) is that it

includes the slot dimension, $\underline{a}$. Equations (7) and (8) show that ϕ becomes more negative as $\underline{a}$ decreases, and from Equation (2) E_x becomes more noble. This strong effect of the crack dimensions on the local solution potential is plotted in Figure 16. It shows that for "sharp" cracks very large (negative) values are to be expected. Thus, the salient point is that this model successfully predicts large (10^2 to 10^3 mV) voltage changes in the x direction for sharp, closed cracks, e.g., $\underline{a} \lesssim 50$ μm for $L = 1$ cm and $i_s = 100$ A m^{-2}, without incorporating constrictions such as gas bubbles in the cavity. For more open cracks or crevices, the 10^{-2} to 10^{-3} mV measured voltage changes can be accounted for by the presence of gas or solid corrosion product in the cavity. Similarly, Equations 8 and 9 show that the concentration and current-density gradients also become steeper as $\underline{a}$ decreases. The former is shown in Figure 17.

The anticipated symmetrical result for anodic polarization, using a model which takes into account the narrowness of the electrolyte path and includes sidewall dissolution, is that the potential gradients, for sharp cracks or narrow crevices, will be steeper than those for more open crevices. The former (for very narrow crevices) are expected to be comparable to those produced in wide crevices or pits containing in-place gas bubbles. This result has been used to explain the observed effect of the magnitude of the crevice opening on the location of the local cell action in a crevice, as illustrated in Figure 12.

4c. Failure of Cathodic Protection Systems

Cathodic protection systems are designed to polarize the metal surface to a potential which is less noble than the equilibrium potential of the metal/solution system. Failure of cathodically protected surfaces, however, can occur for a number of reasons. One of these is that crevices or cracks exist in the surface, and have their own surfaces that are exposed to the environment and, therefore, also require protection by the system. Based on the results of

the modeling in Section 4b, the narrower the crevice or crack the more sharply the electrode potential shifts in the more noble direction with increasing distance into the cavity and, hence, the less effective will be the cathodic protection of the crevice walls. Furthermore, the h.e.r. typically occurs during cathodic protection of steel and other base metals. Hence, gas accumulation in the cavity can be expected, making cathodic protection of the crevice walls even less effective. Thus, both narrowness of the crevice and gas accumulation in it, produce steep gradients of the electrode potential within the cavity, and the concommitant loss of cathodic protection within most of the cavity. The polarization condition given below in Figure 19b illustrates this loss of protection within cavities.

4d. The Limiting Potential, E_{LIM}

The application of the concept of a limiting potential, E_{LIM}, within a cavity is a recent development (19, 20). The change in electrode potential with distance x into the cavity, E_x, is given by Equation (2). Substituting the IR voltage, that exists along the column of electrolyte which fills the cavity, for ϕ_x one obtains

$$E(x) = E_{x=o} + IR(x) \qquad (11)$$

where I is the current flowing in or out of the cavity with due regard for the current flow direction, and R(x) is the resistance to current flow between x=0 and position x. Eq. 11 shows that I must be finite or IR=0 and $E(x) = E_{x=0}$. Thus, I can be very small if R is very large and still produce a large IR, e.g., due to in-place gas bubbles, but even for R $\rightarrow$ ∞ the IR product is zero if I goes to zero. It follows since the current I decreases with decrease in the overpotential, that E_{LIM}, in principle, corresponds to the approach (decrease)

of the current, I, flowing in or out of the cavity, to zero in the limit.

The above criteria defining E_{LIM} assumes a simple situation in which the current I comes mainly from a local cell, e.g., from the tip of a crack where the reaction is metal dissolution. For most electrode and many corrosion processes, e.g., oxygen or hydrogen evolution and metal dissolution along the walls of a crevice, however, the reaction will be distributed along the walls of the cavity and the reaction rate will decrease with increasing distance x into the cavity. The latter occurs because $IR(x)$ in Equation (11) increases, corresponding to a decreasing overpotential, i.e., $E(x)$ changes in the direction of E^{eq}, with increasing x. Thus, the limiting current condition is relaxed and becomes one of zero-current flow beyond some depth, rather than zero current flow in or out of the cavity. Then, the local current is essentially zero at some depth x and beyond, corresponding to the E_{LIM} condition, and both the integrated current flowing into the cavity and the IR term in Equation (11) are finite. This situation is illustrated above for crevicing in Figure 12 for which the E_{LIM} condition defines one of the boundaries of the local cell, that furthest from the crevice mouth.

For a single reaction occurring in the cavity, the above defined zero current flow condition corresponds to the equilibrium electrode potential for the reaction producing the current I, as shown in Figure 18. A single reaction, metal dissolution, could occur in a pit in a noble metal with the outer surface (x=0) in the passive region, Figure 18a, or hydrogen evolution could occur within a crack, as well as at the outer surface of a noble metal, Figure 18b. E_{LIM} for these examples is then the equilibrium potential (for the local composition of electrolyte in the cavities) of the respective reactions, metal dissolution (Figure 18a) or hydrogen evolution (Figure 18b). Figure 18a describes the situation when $E_{x=0}$ is established either by an external power

supply or by a suitable oxidant undergoing reduction at the outer surface as part of an open circuit corrosion process.

If a second reaction, of opposite sign to the reaction producing the current I, occurs in the cavity, the zero current-flow condition corresponds to the mixed potential of the two reactions (or of multiple reactions) occurring in the cavity, rather than the equilibrium potential of the primary reaction, as shown in Figure 19. This situation exists for the large IR voltages, described above during pitting in iron and other base metals, that places E_x (Equation 11) in the region of the h.e.r. (Figure 19a). Similarly, E_x within a crack during electroplating or cathodic protection can be in the region of anodic dissolution of the metal being plated or protected, respectively (Figure 19b).

If two or more reactions, of the same sign, occur in a cavity, E_{LIM} corresponds to the equilibrium potential of the thermodynamically most favored reaction. Thus, for oxidation reactions, E_{LIM} is the most negative (least noble) equilibrium potential since it, but not the others, corresponds to the zero-current condition (19, 20).

Some experimental results consistent with the concept of a limiting potential are (1) the leveling off of the electrode potential beyond some distance x into the cavity in Figure 14, and (2) the absence of metal dissolution along the walls of the slot in the Cu sample during the h.e.r., whereas metal dissolution is observed for the same conditions in the base metals, Fe and Ni. According to the E_{LIM} concept, copper cannot dissolve because $E_{LIM} = E_{H/H+}^{eq} < E_{Cu/Cu++}^{eq}$.

5. DISTINGUISHING BETWEEN HYDROGEN CRACKING AND SCC

Two recent developments, when applied to aqueous cracking situations in the noble metals, provide a definite answer to the question (20): Will (or did) failure occur due to hydrogen cracking or due to anodic (metal dissolution)

stress corrosion cracking? These are (1) the E_{LIM} concept and (2) the relative
change in concentration of certain of the ionic species with increasing distance
x into the crack (actual concentrations are not needed).

Noble metals are chosen for the analysis because one can say with a high
degree of certainty that there is no overlap at the outer surface of the
potential regions of anodic metal dissolution and the h.e.r. It follows because
of the existence of the E_{LIM} potential, that only one form of cracking can be
initiated at the outer surface depending on the mode of polarization. For
anodic polarization (including open circuit corrosion), only anodic metal
dissolution is possible (at the outer surface); and for cathodic polarization
only hydrogen evolution and hydrogen cracking are possible. Thus, this is a
good starting point for asking what is the equivalent situation at the tip of a
preexisting crack or cavity in the noble metal sample. The answer is that if
the polarization curves do not overlap, i.e., the equilibrium potentials move
farther apart, rather then closer together, with increasing distance x into the
cavity, only one form of cracking is possible anywhere in the cavity for a given
polarization mode, anodic or cathodic.

The changes in ionic concentration with distance x are shown in Figures 20
and 21 for anodic and cathodic polarization of copper in perchloric acid,
respectively. For anodic polarization and considering copper dissolution occurs
only at the bottom of the cavity, the pH and Cu^{++} and ClO_4^- ion
concentrations increase with increasing x. From the Nernst equation, the
equilibrium potentials of the hydrogen and copper reactions decrease and
increase, respectively, with increasing x. Similarly, for cathodic polarization
of the Cu (Figure 21), the pH increases. The latter produces a shift of the
equilibrium potential for the h.e.r. in the negative potential direction. As
some Cu^{2+} ions initially form by dissolution (since the bulk solution had

none), their concentration also increases with distance into the cavity, under the influence of the solution potential which decreases with increasing x (20), in which case the copper equilibrium potential becomes more positive with increasing distance into the cavity. Thus, for either anodic or cathodic polarization conditions, the possibility of overlap of the two electrode potential regions decreases, rather than increases, with increasing distance x into the cavity, as illustrated in Figure 22. Since for non complexing solutions there is no overlap at the outer surface, it follows from the E_{LIM} concept that for either polarization mode, there is no value of the electrode potential which would allow both the h.e.r. and metal dissolution to occur at the crack tip. Note, that for these answers to the questions of overlap and cracking mode in noble metals, it was not necessary to determine the actual ionic concentrations in the crack. The trends of ionic concentration in Figures 20 and 21 are well established based on mass and charge transport models and experimental data (10, 12, 21). These trends persist from time zero and become more, rather than less, pronounced in the presence of constrictions such as gas accumulation.

It follows that crack propagation during anodic polarization (of noble metals in solutions for which overlap does not occur at the outer surface) is not due to hydrogen and, similarly, during cathodic polarization is not due to anodic metal dissolution. Table 4 lists known cases of cracking in noble metal alloys. In those cases of cracking during open circuit corrosion (OCP), the measured corrosion potential was in the potential region of metal dissolution by virtue of the addition to the electrolyte of a strong oxidant, e.g., HNO_3 or ferric ion, in which case it was clear that the open-circuit condition was equivalent to anodic polarization. Hence, all cases of cracking in Table 4 are for anodic polarization; therefore, none of these failures can be attributed to

hydrogen, and in turn all must be due to an anodic type process such as metal dissolution.

For base metals or alloys containing base metals, the above analysis can not rule out one or the other mode of cracking since, in general, the anodic and cathodic polarization curves overlap at the surface of the sample, and also, to at least some extent, within the crack even though the polarization curves may diverge with increasing x. An example is α-brass, which has a long history of environmental cracking and continues to be the focus of mechanistic studies in many laboratories. The least noble metal is Zn, and its polarization curve and

Table 4. The mode of cracking (SCC or HC) based on the E_{LIM} criterion for known cases of crack propagation in noble metal alloys for the reported mode of polarization.

Alloy	Solution	Mode	SCC or HC	Ref
Cu-18a/o Au	H_2SO_4 (dil.)	anodic	SCC	22
	or KCl*	anodic	SCC	22
	or $FeCl_3$*	OCP+	SCC	22
Cu-25a/o Au	$FeCl_3$	OCP	SCC	23
Cu-25a/o Au	1M H_2SO_4	OCP	SCC	24
Cu-40a/o Au ·	Ce^{4+} ions	OCP	SCC	24
Ag-20a/o Au	HNO_3	OCP	SCC	25
	or $FeCl_3$*			
Ag-15a/o Pd	Aqua Regia	OCP	SCC	26
	or $FeCl_3$*			

+OCP (open circuit potential)

*Neutral solutions for which (i) overlap does not occur at the outer surface

even though Cu complexes with chloride ion and (ii) similar calculations, to those that produced Figures 20 and 21 for acid solution, also show the trend in Figure 22.

that of the h.e.r. overlap even at neutral and higher pH. The E_{LIM} values in this case are the mixed potentials of these two reactions established within the crack during either an anodic or cathodic polarization process (Figure 19). Thus, for anodic polarization and $E_{x=L}$ near E_{LIM} (Equation 11), both Zn dissolution and hydrogen discharge can occur at the crack tip making it impossible to eliminate either cracking mode from consideration (20). Similarly, during cathodic polarization with $E_{x=L}$ in the range between $E_{Zn/Zn^{++}}^{eq}$ and E_{LIM} both Zn dissolution and the h.e.r. can occur at the crack tip. In conclusion, both forms of cracking can occur for either cathodic or anodic polarization in base metal or mixed base/noble metal alloys. As such these alloys are not as suitable (as noble metal alloys) for studying certain fundamental aspects of the mechanism of stress corrosion or hydrogen cracking.

6. CONCLUSIONS

. This talk reviews work in the author's laboratory on corrosion products in cavities beginning with the finding that "wedging" action can occur and produce stress corrosion cracking and degradation of steel-reinforced concrete.

. Hydrogen gas readily forms and accumulates within cavities in base metals during localized corrosion or cathodic protection.

. The potential at the cavity or crack tip can be much different than at the outer surface during anodic or cathodic polarization or open circuit conditions when

. gas is present in the cavity, or

. a dimension of the cavity opening is small compared to its depth, as is generally the case for hydrogen cracking or SCC

. The local electrode potential within pits and crevices is the primary parameter (i) promoting pit growth and crevicing, and (ii) when combined with compositional effects, in establishing their growth rate. During cathodic polarization the electrode potential within the cavity determines the effectiveness of cathodic protection of the cavity (crack) surfaces.

. Anodic stress corrosion cracking and hydrogen cracking can be separated by judicious choice of conditions in the case of noble metal alloys.

ACKNOWLEDGEMENTS

Frankenthal, P. J. Byrne, J. E. Holliday, B. G. Ateya, T. Sakurai, I. M. Bernstein, S. S. Chatterjee, W. R. Bitler, J. E. Castle, G. K. Hubler, A. M. Allam, H. Erhart, R. Raicheff, R. P. Das, H. J. Grabke, J. H. Hoke, K. Osseo-Asare, A. Jimbo, H. Kim, G. C. Ye, T. T. Kam, C. M. Loxton, I. S. T. Tsong, M. N. Desai, K. Murakami, T. Hashizume, T. Abe, T. Suzuki, K. Weil, and R. Iyer. Students Y. S. Kim, A. Lingras, M. Zamanzadeh, Y. Kuk, C. Kato, B. W. Bennett, A. K. Birchenall, K. Al-Saleh, D. R. Hess, S. Kaja, H. S. Kim, H. Shih, J. D. Fritz, H. P. Hack, A. Valdes, Y. T. Kho, P.Cronmiller, W. S. Aaron, G. E. Williams, D. Harris, R. D. Walsh, K. W. Rosengarth, D. Marx, I. Takeuchi, J. D. Katz, H. J. Wei, J. Lee, M. El-Maazawi, D. R. Moyle, J. W. Hyres, M. H. Tosten, G. M. Carinci, D. P. Hohman, B. C. Thomas, J. St. John, and K. J. Fioravanti.

Figures 5 and 6 of the paper, "On the Mechanism of Localized Corrosion of Iron and Stainless Steel," H. W. Pickering and R. P. Frankenthal, J. Electrochem. Soc., 119, 1297 (1972), Figure 3 of paper II of this series, R. P. Frankenthal and H. W. Pickering, J. Electrochem. Soc., 119, 1304 (1972), and Figures 1, 5, and 7 of the paper "On the Nature of Electrochemical Reactions at a Crack Tip During Hydrogen Charging of a Metal," B. G. Ateya and H. W. Pickering, ibid., 122, 1018 (1975) were reprinted by permission of the publisher, The Electochemical Society, Inc.

REFERENCES

1. N. A. Nielsen, "The Role of Corrosion Products in Crack Propagation in Austenitic Stainless Steel: Electron Microscope Studies," in Physical Metallurgy of Stress Corrosion Fracture, T. Rhodin, ed., pp. 121-146, Interscience Publishers, New York (1959).

2. H. W. Pickering, F. H. Beck and M. G. Fontana, "Wedging Action of Solid Corrosion Product During Stress Corrosion of Austenitic Stainless Steels," Corrosion, 18, 230t-239t (1962).

3. J. H. Hoke, H. W. Pickering and K. Rosengarth, "Measurement of Stresses Developing During Corrosion of Embedded Concrete Reinforcing Bars," TMS Paper F81-6, Symposium on Degradation of Materials, The Metallurgical Society of AIME, Warrendale, PA (1981).

4. G. Herbsleb and H. J. Engell, Z. Elektrochem., 65, 881 (1961).

5. N. D. Greene, W. D. France, Jr., and B. E. Wilde, Corrosion, 21, 275 (1965).

6. C. M. Chen, F. H. Beck, and M. G. Fontana, Corrosion, 27, 234 (1971).

7. P. Forchhammer and H. J. Engell, Werkstoffe und Korrosion, 20, 1 (1969).

8. G. Masing and D. Altenpohl, Z. Metallk., 43, 433 (1952).

9. H. Kaesche, Z. Physik. Chem. N. F., 26, 138 (1960); ibid., 34, 87 (1962).

10. H. W. Pickering and R. P. Frankenthal, J. Electrochem. Soc., 119, 1297 (1972); ibid., "Mechanism of Pit and Crevice Propagation on Iron and Stainless Steels" in Localized Corrosion, R. W. Staehle, B. F. Brown, G. Kruger and A. Agrawal, eds., pp. 261-269, National Association of Corrosion Engineers, Houston, Texas (1975).

11. R. P. Frankenthal and H. W. Pickering, J. Electrochem. Soc., 119, 1304 (1972).

12. B. G. Ateya and H. W. Pickering, J. Electrochem. Soc., 122, 1018 (1975).

13. D. Harris, M.S. Thesis, The Pennsylvania State University, 1975.

14. D. Harris and H. W. Pickering, "On Anodic Cracking During Cathodic Hydrogen Charging" in Effect of Hydrogen on the Behavior of Materials, A. W. Thompson, I. M. Bernstein and A. J. West, ed., pp. 229-231, AIME, Warrendale, PA (1976).

15. A. Valdes and H. W. Pickering, to be published.

16. R. P. Frankenthal and H. W. Pickering, J. Electrochem. Soc., 120, 23 (1973).

17. H. Miyuki, Sumitomo Metal Industries, Ltd., Central Research Laboratories private communication, 1985.

18. C. Wagner, Plating, 48, 997 (1961).

19. H. W. Pickering, "The Limiting IR Voltage Within Electrolyte in Cavities During Localized Corrosion and Hydrogen Charging of Metals," in H. H. Uhlig Symposium, Corrosion and Corrosion Protection, R. P. Frankenthal and F. Mansfeld, eds., pp. 85-91, The Electrochem. Soc. Inc., Pennington, NJ, 1981.

20. H. W. Pickering, "On the Limiting Electrode Potential in Cavities and Its Role in Deciding Between SCC and HC in Metals," in <u>Intern. Congress on Metallic Corrosion (9th)</u>, Vol. 2, pp. 246-253, National Research Council Canada, Ottawa, Ontario, 1984.

21. B. G. Ateya and H. W. Pickering, J. Appl. Electrochemistry, <u>11</u>, 453 (1981).

22. H. Gerischer and H. Rickert, Z. Metallkunde, <u>46</u>, 681 (1955).

23. R. Bakish and W. Robertson, Trans. AIME, <u>206</u>, 1277 (1956).

24. H. W. Pickering, Corrosion, <u>25</u>, 289 (1969).

25. L. Graf and J. Budke, Z. Metallkunde, <u>46</u>, 378 (1955).

26. L. Graf, "Stress Corrosion Cracking in Homogeneous, Non-Supersaturated Alloys Containing Noble or No Noble Metals" in <u>Fundamental Aspects of Stress Corrosion Cracking</u>, R. W. Staehle, A. J. Forty and D. van Rooyan, eds., pp. 187-201, National Association of Corrosion Engineers, Houston, Texas (1969).

FIGURE CAPTIONS

Figure 1. (Top) Stress corrosion cracks at the base of the circular notch in Type 347 stainless steel due to solid corrosion product formation between the plate and the notch walls (2X) and the transgranular nature of the cracks (100X) (2).

Figure 2. Propagation by wedging action of a pre-existing crack (top left) from A to the right upper surface (2).

Figure 3. Cyclinder expansion, due to wedging action, vs. exposure time in the autoclave at 204°C. Insert shows austenitic stainless steel sample and titanium cyclinder as components (left) and assembled (2).

Figure 4. (Top) Specimen design for simulating wedging action in steel reinforced concrete, and average measured strain of the titanium versus time in the solution (3).

Figure 5. Pitted specimen, microscope, and microprobe and micromanipulator for measuring the electrode potential inside the pits.

Figure 6. Pits in an iron sample (top left and right), and four consecutive frames of a movie showing a bubble (and mirror image) rising out of one of the pits. Anodically polarized in 0.5M H_2SO_4, 3 mM NaCl (pH = 0.3) (10,11).

Figure 7. In-place hydrogen gas bubbles inside the slot, that formed during cathodic polarization at 9 A m^{-2} in the pH 5 solution, photographed through a transparent plastic used to form the slot with the Fe (13,14).

Figure 8. Wall of the slot in an Fe sample that is heavily corroded where the hydrogen gas bubble had been in contact with the iron during anodic polarization (15).

Figure 9. Schematic illustration of the electrode potential behavior as a function of (a) distance into the pit or crevice and (b) time at the site of the local cell.

Figure 10. Matching segments of the measured current flowing out of a single pit and the measured electrode potential near the bottom of the pit, as a function of time (10).

Figure 11. The various schemes for stabilization of pit and crevice growth, illustrating the effect of (a) potential, (b) chloride ion, (c) acidification, (d) potential and Cl$^-$ ion and (e) potential and acidification. Dashed lines illustrate the effect of composition change on the polarization curve inside the cavity.

Figure 12. Effect of crevice dimension a on the location of the local cell action along the x direction of the crevice. $E_{A/P}$ is the potential of the active/passive transition.
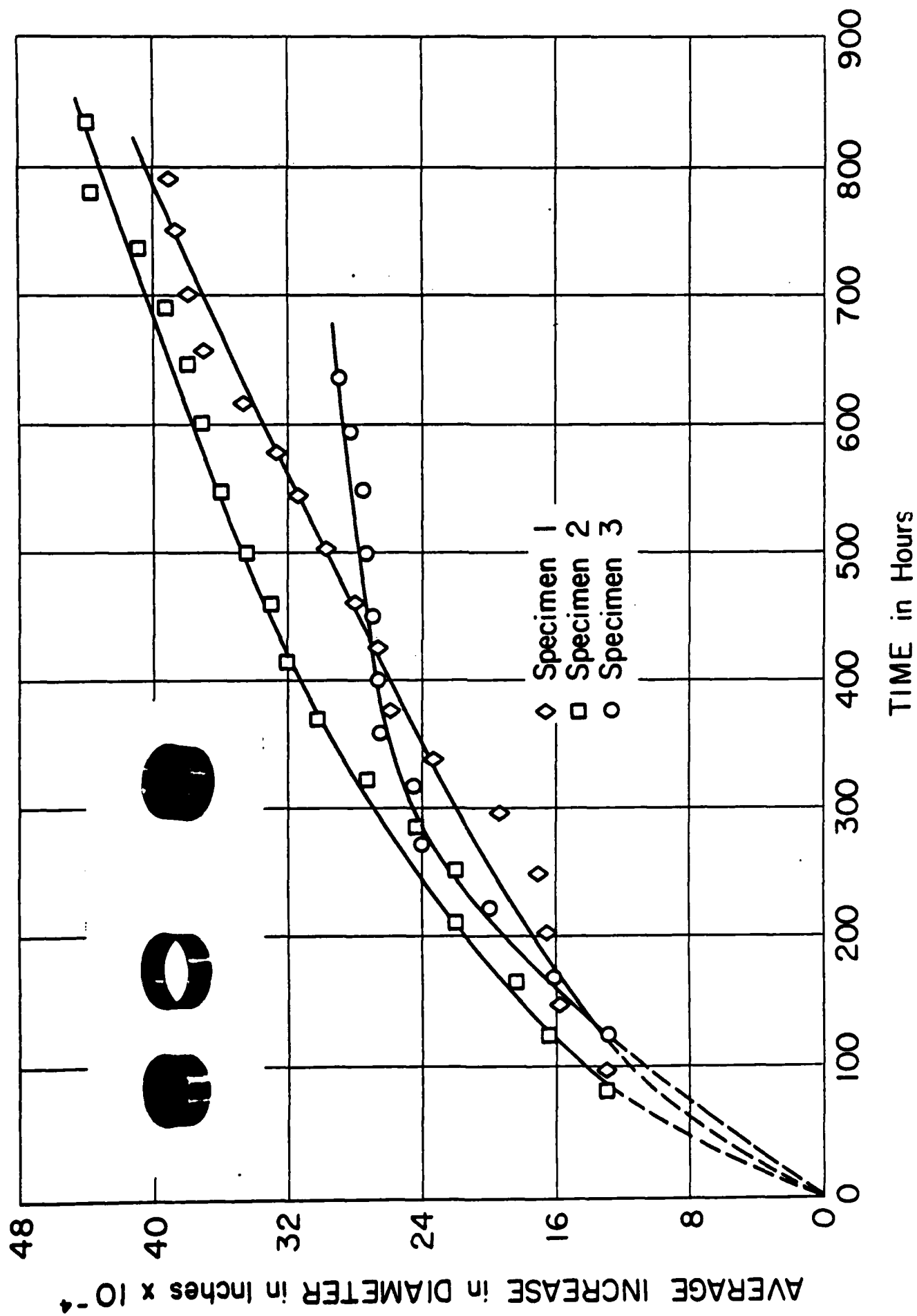
Figure 13. Model of a crack (12).

Figure 14. The potential change, ϕ, within the slot electrolyte of an iron sample, for the h.e.r. at 52 A m^{-2}. $\underline{a}$ = 0.05 cm. Points are for traverse of the Luggin probe into (o) and out of ($\square$) the slot. Time of traverse was 25 min. The calculated ϕ profile is from Equation (8); X = 0.3 cm (12).

Figure 15. An example of etching of the wall of the slot in an Fe sample during the h.e.r. for which the outer surface is in a state of complete cathodic protection. Location of etching is where the H$_2$ gas had accumulated (14).

Figure 16. Calculated ϕ potential for increasing distance x into a slot of depth L = 1 cm, illustrating the effect of the slot dimension $\underline{a}$ (Figure 13) for i_s = 100 A m^{-2} (12).

Figure 17. As in Figure 16 but for the concentrations of hydrogen ion and the anion, which are the same for the particular model conditions.

Figure 18. E_{LIM} for the case of a single reaction in the cavity. (a) Anodic polarization. (b) Cathodic polarization. Dashed and solid lines indicate the E-i curve is for the x = L and x = 0 locations, respectively (19,20).

Figure 19. E_{LIM} for the case of a second reaction of opposite sign in the cavity. (a) Anodic polarization. (b) Cathodic polarization. Dashed and solid lines indicate the E-i curve is for the x = L and x = 0 locations, respectively (19,20).

Figure 20. Quasi stationary concentration profiles for steady state copper dissolution at the bottom of a pit. Electrolyte is perchloric acid. Calculation method is in Reference 10.

Figure 21. Stationary concentration profiles of H$^+$ and ClO$_4^-$ ions for steady state hydrogen discharge on the sample surface and slot walls. System is copper in perchloric acid. Calculation method is in Reference 12.

Figure 22. Schematic illustration of an increased separation of $E_{M/M^{z+}}^{eq}$ and E_{H/H^+}^{eq} with increasing distance x into the crack and, therefore, no chance of overlap of their respective polarization curves. Dashed lines are for the outer surface position (x = 0) for Cu in a non-complexing aqueous electrolyte (20).
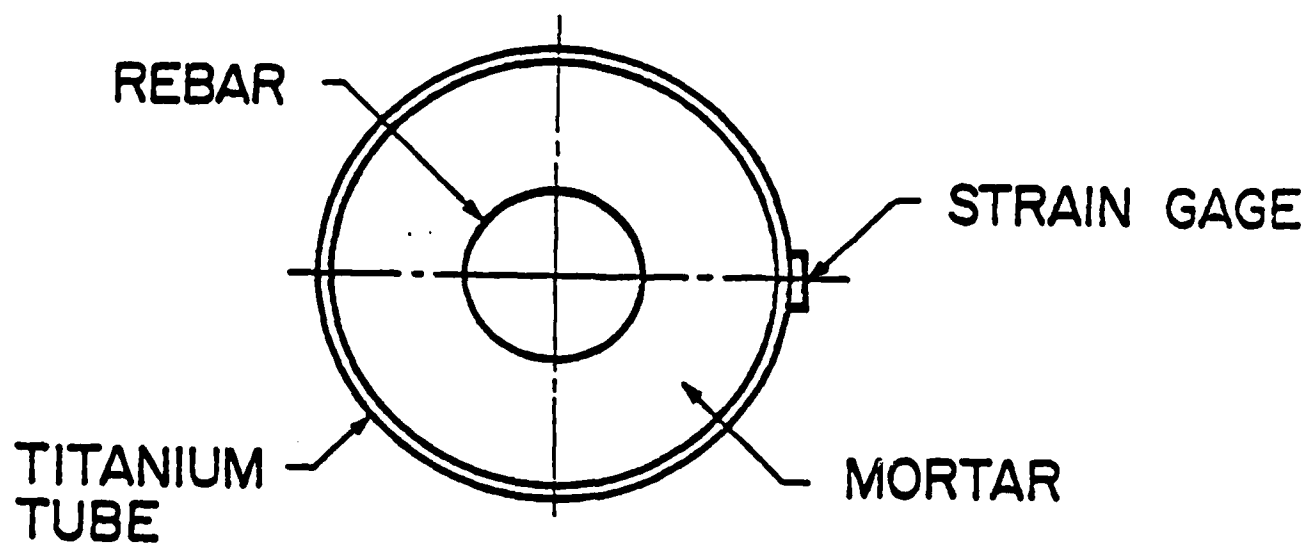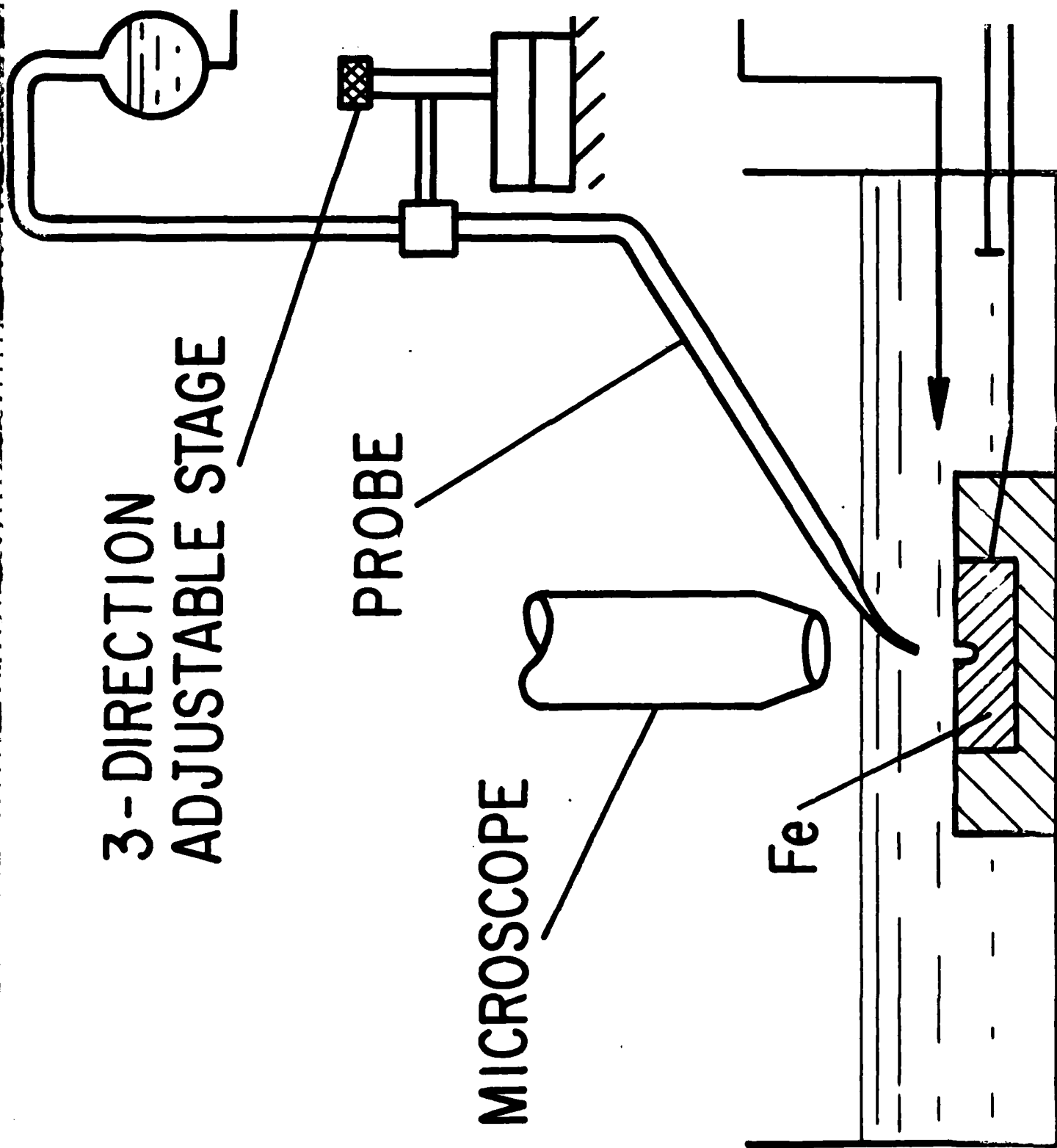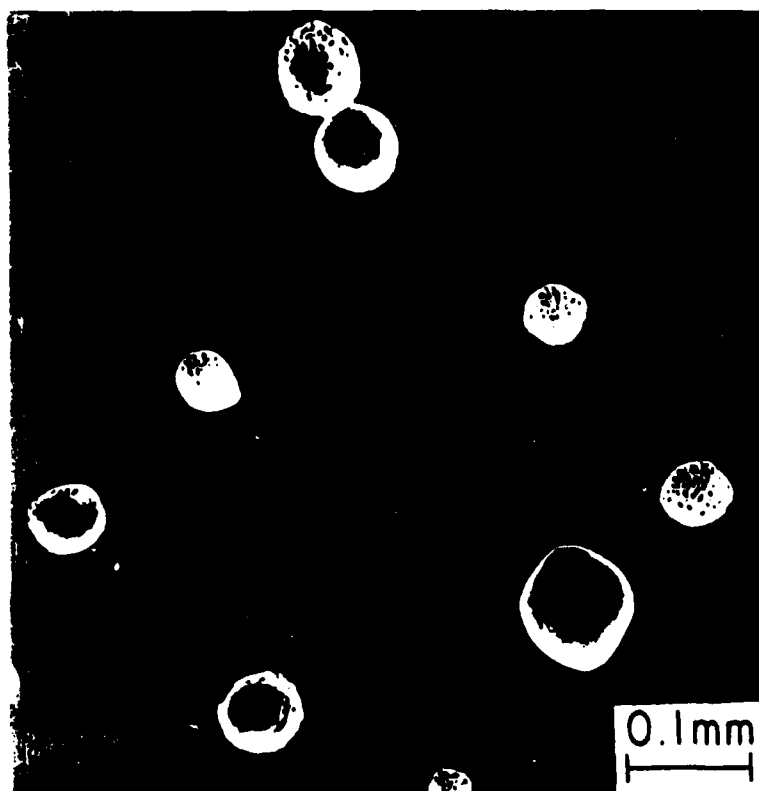
$\sigma_{APPLIED}$

$\sigma_{WEDGING}$

A

0.3mm

AVERAGE INCREASE in DIAMETER in inches x 10⁻⁴

TIME in Hours

Specimen 1
Specimen 2
Specimen 3

REBAR

STRAIN GAGE

TITANIUM TUBE

MORTAR

6.0 V

1.5 V

Potential Applied

Δ STRAIN, microinches/inch

TESTING TIME, DAYS

FIG 4 PICKERING
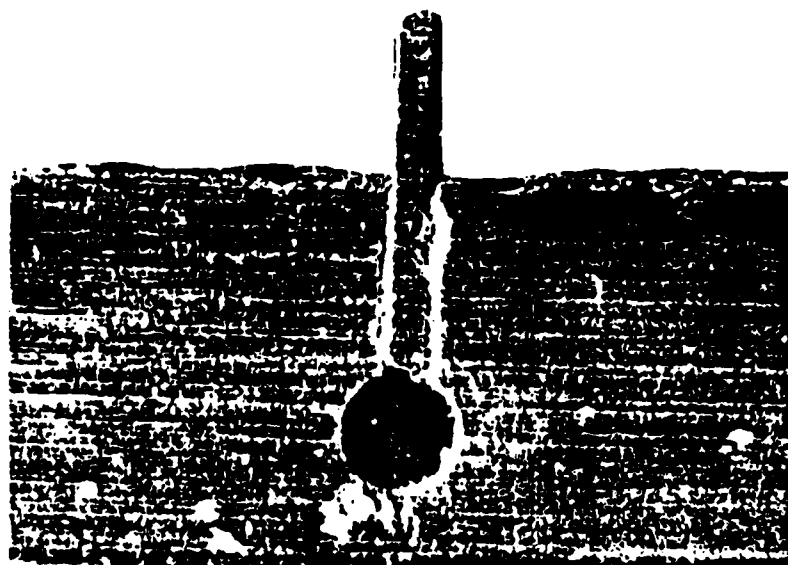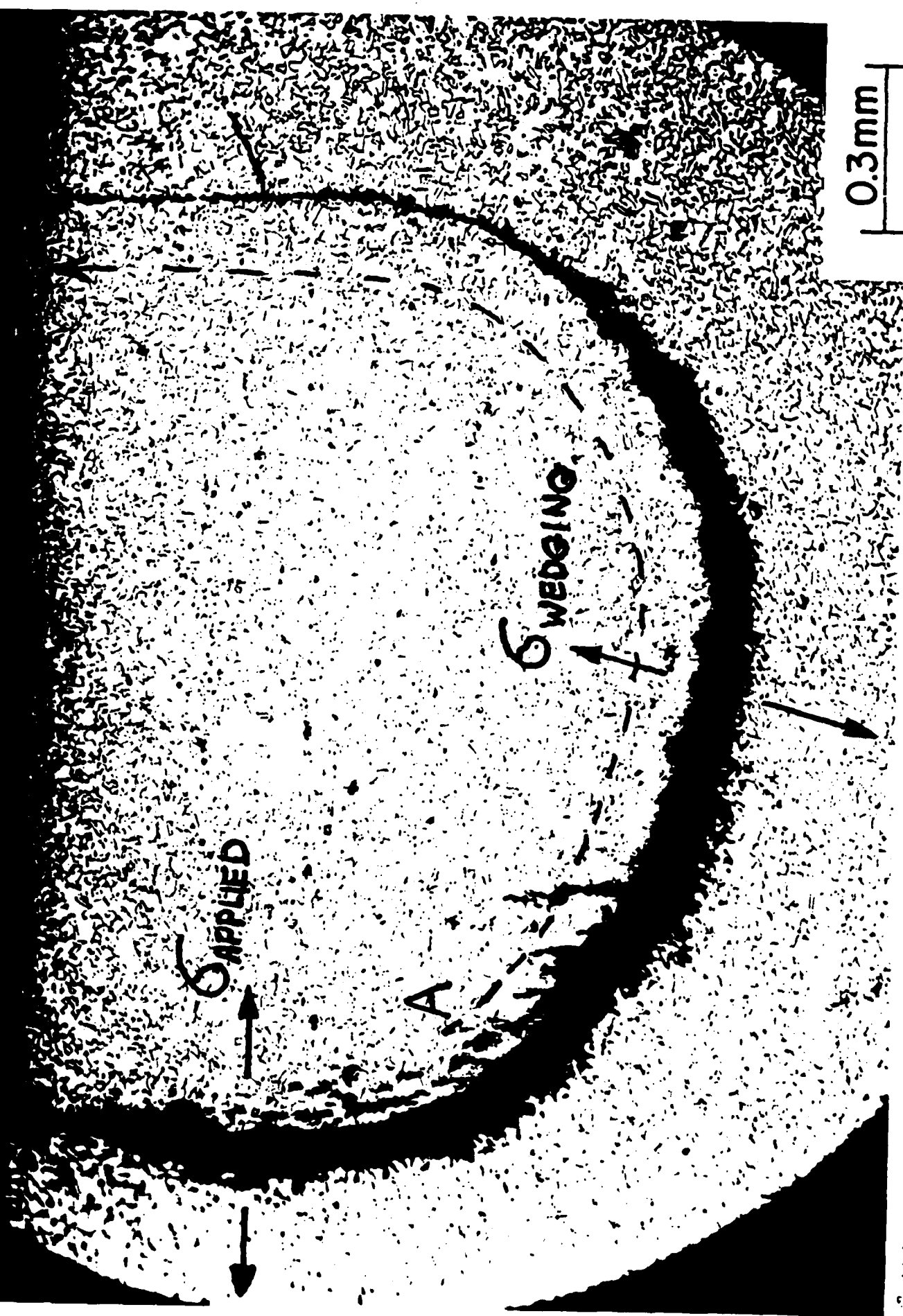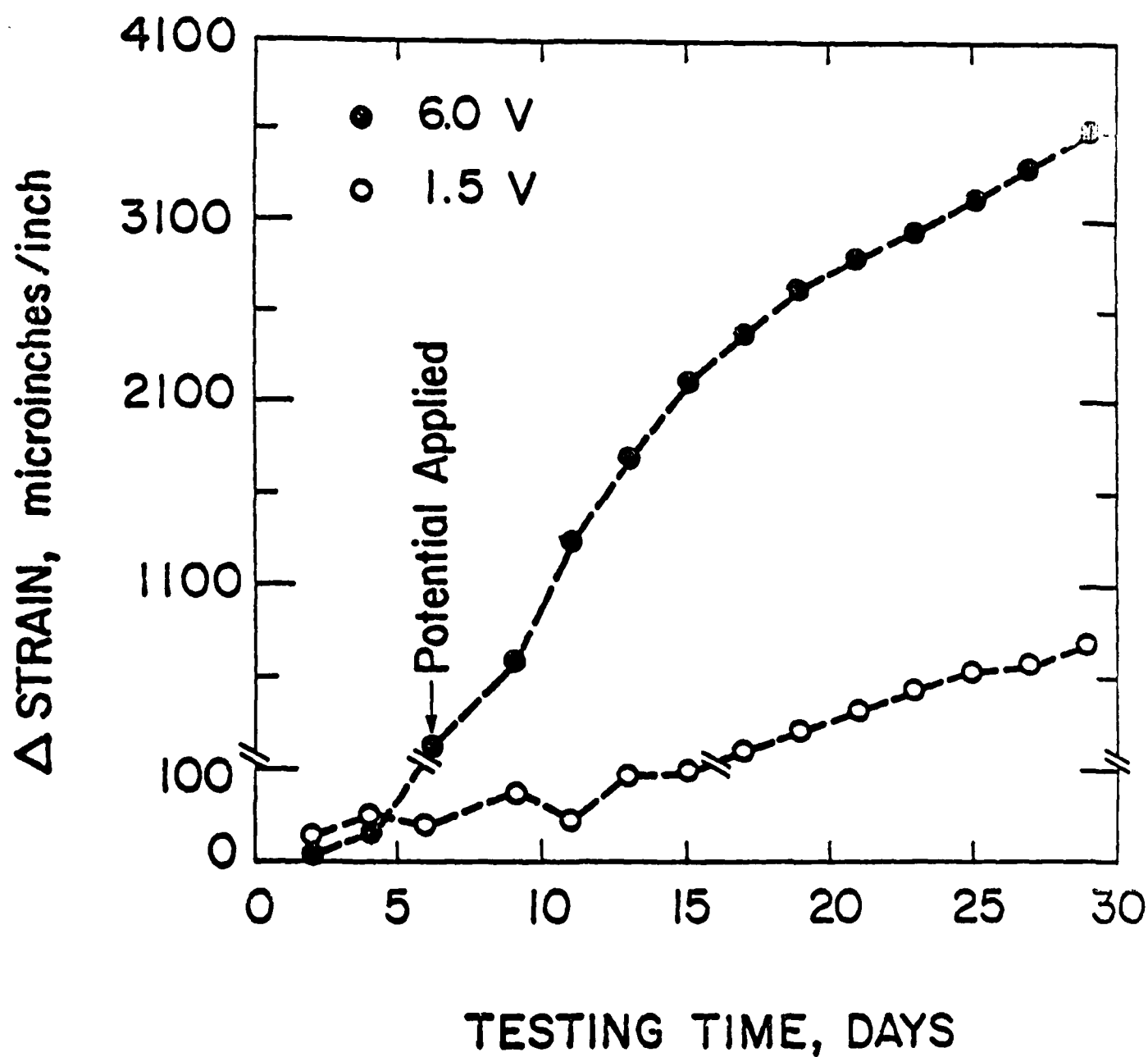
3-DIRECTION ADJUSTABLE STAGE

PROBE

MICROSCOPE

Fe
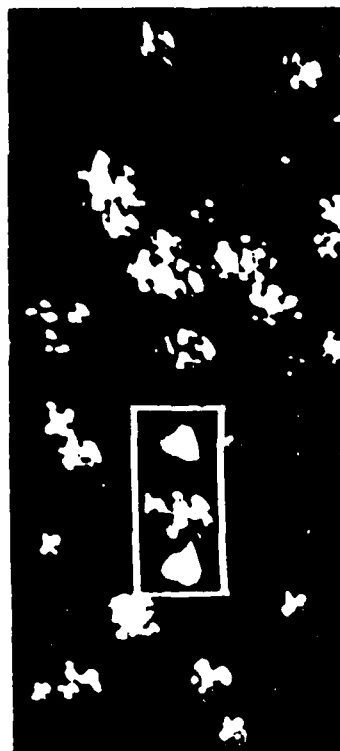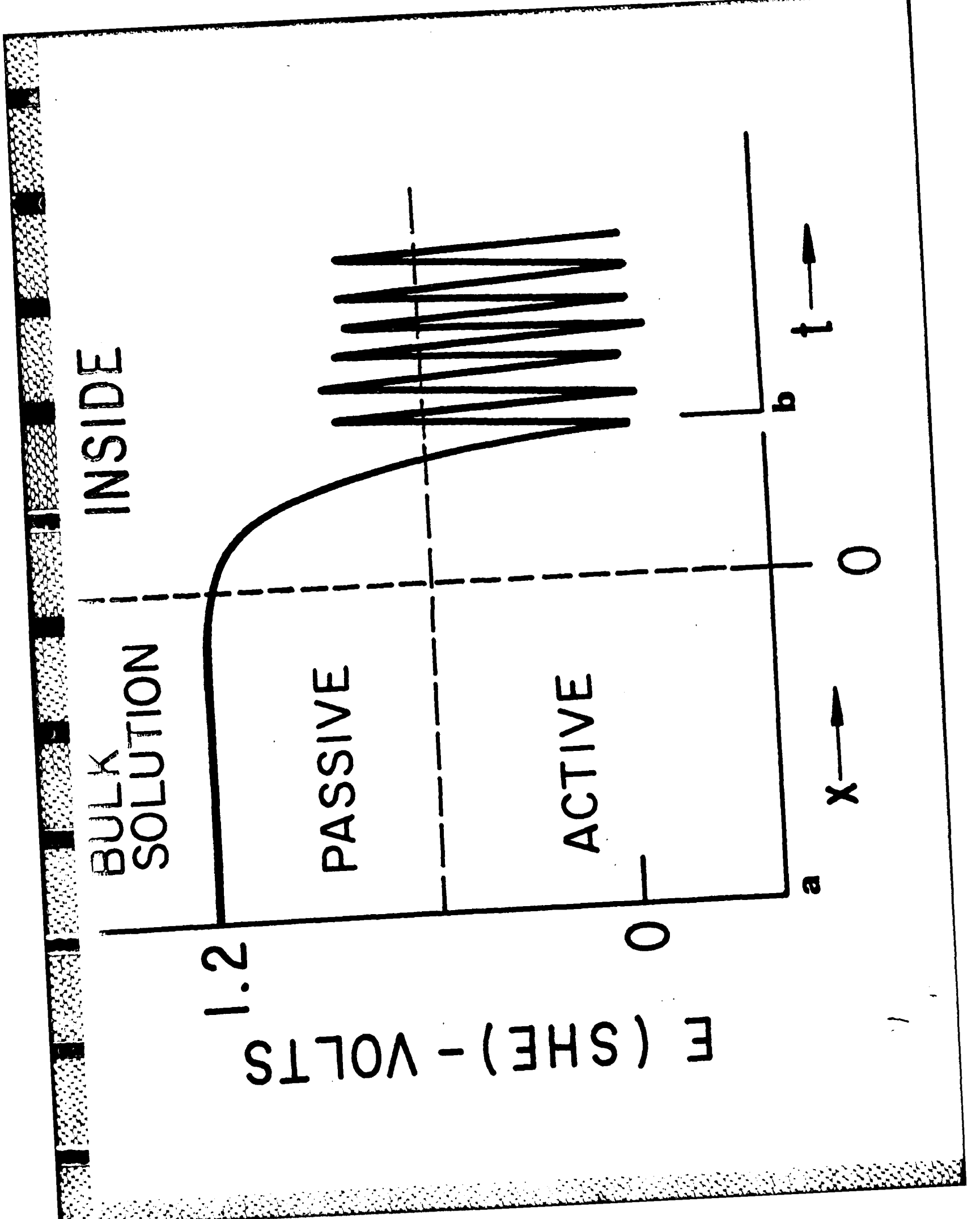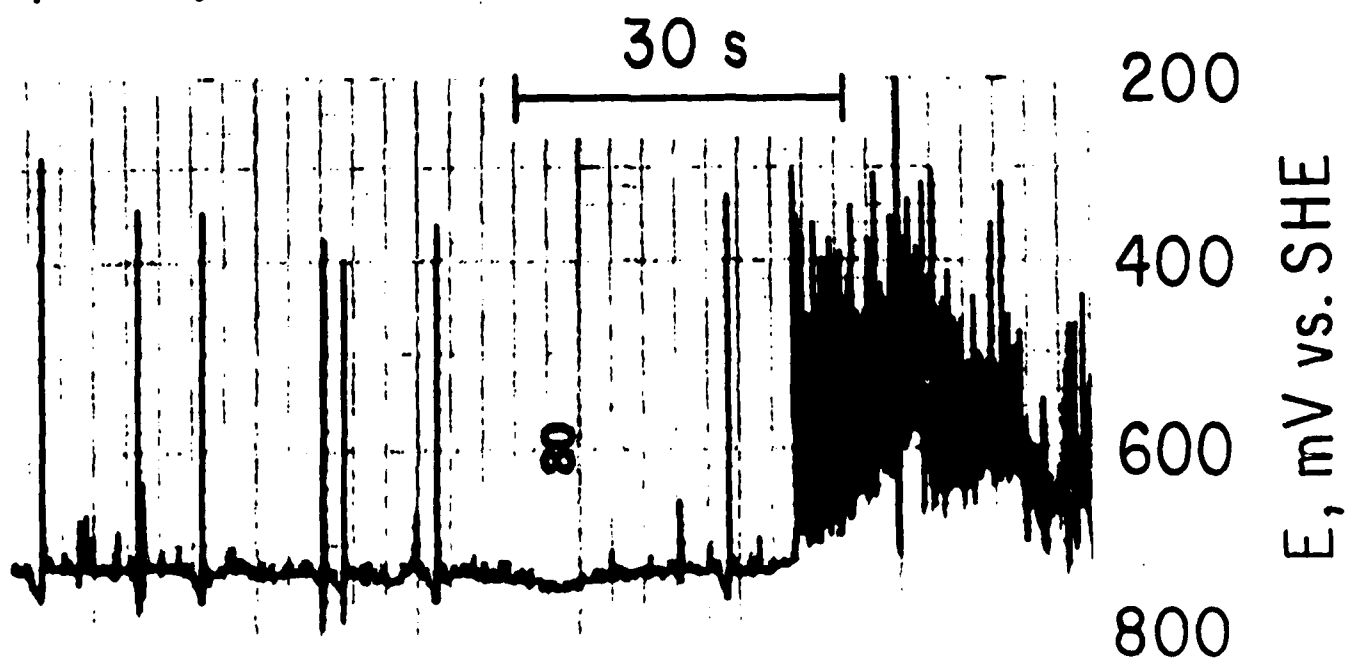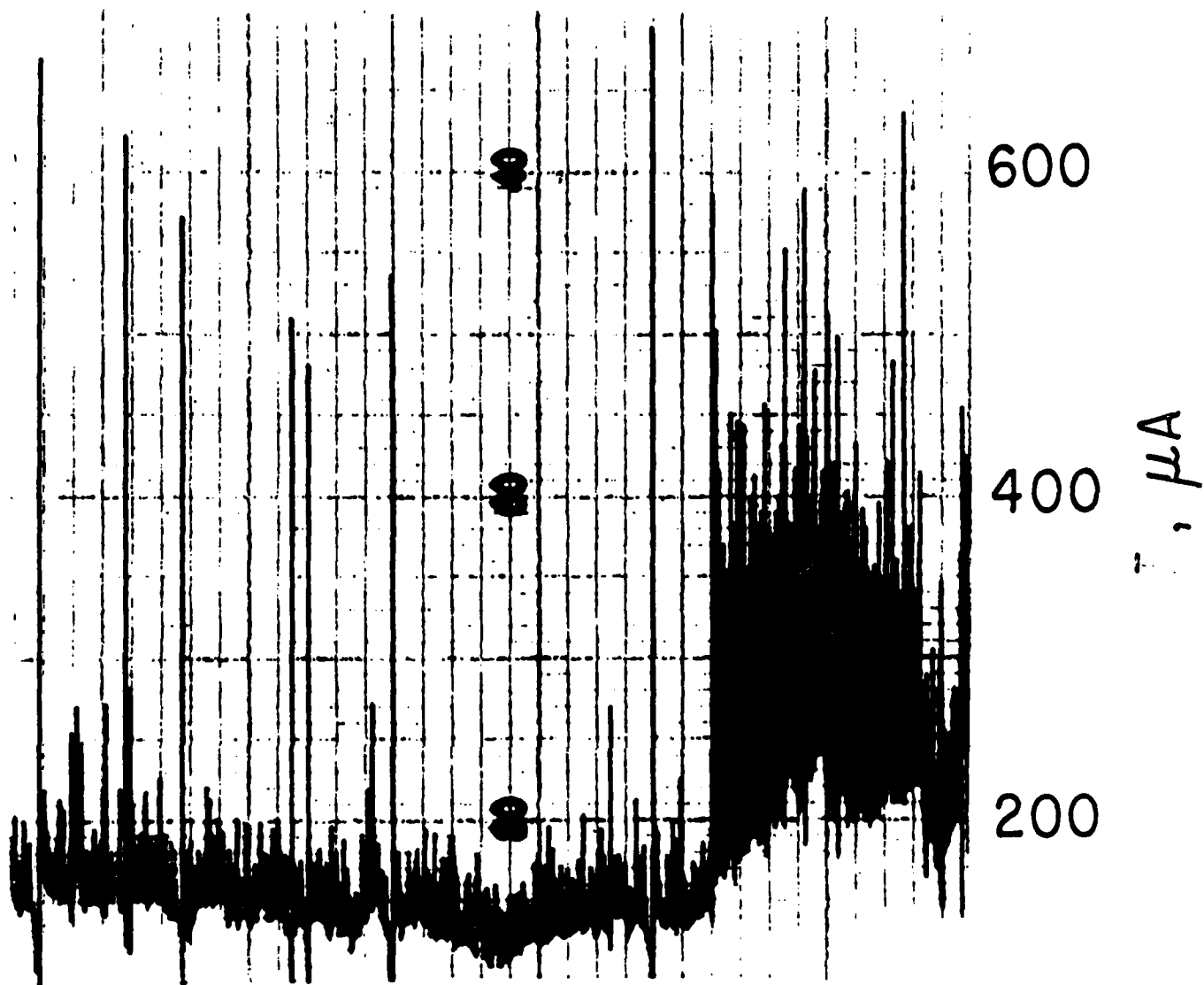
0.1mm   40μm

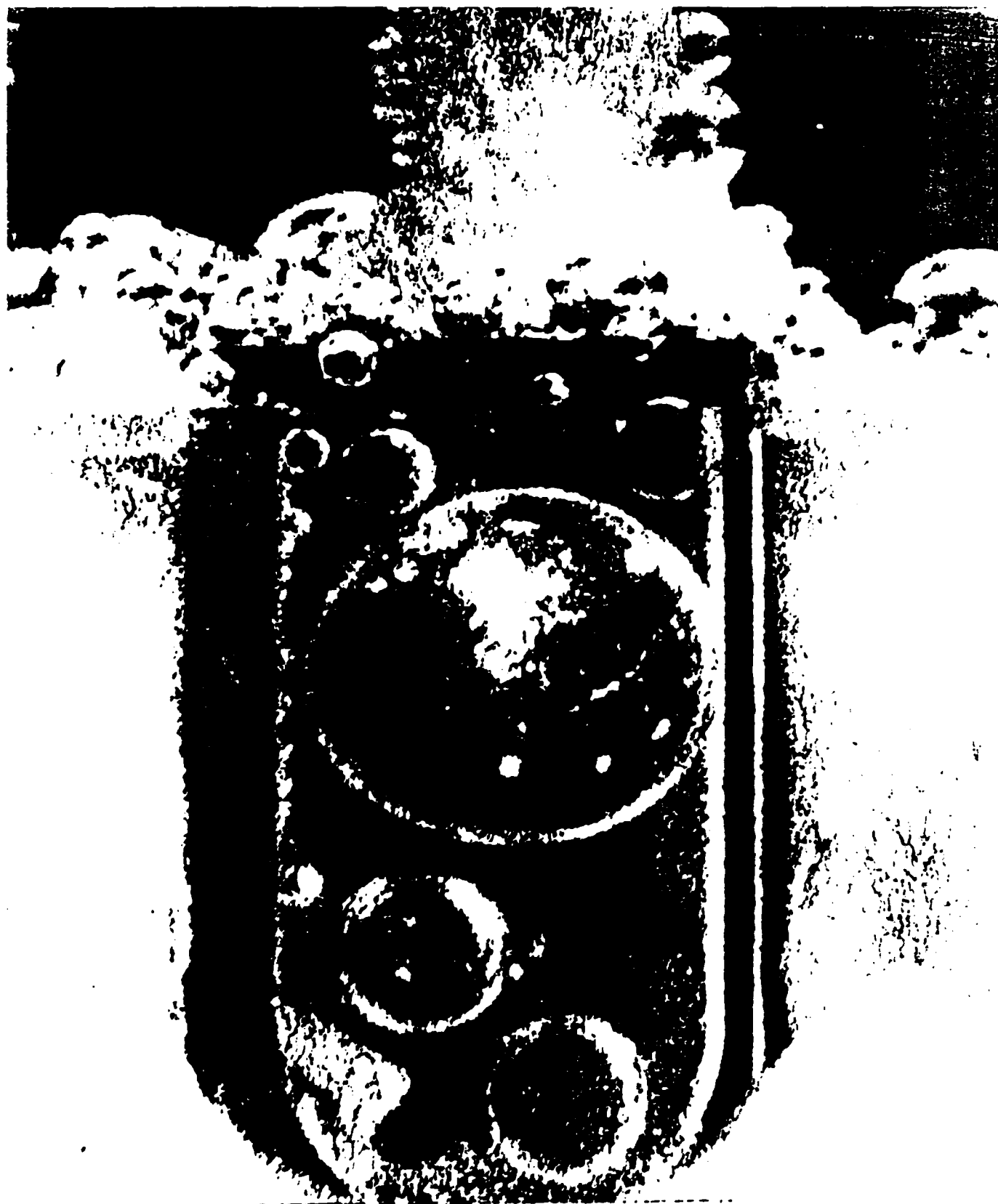a   b   c   d

FIG 6 PICKERING

0.5 cm

FIG. 7. PICKERING

Fig. 8 Prefix...

... ...   96 NNC

POTENTIAL SHIFT

E_{LIM}

$E_{A/P}$

$\log i$

ϕ

E_{SURF}

(a)

$E_{CAV(x,t)}$

COMPOSITION CHANGE

$\uparrow Cl^-$

$\log i$

E_{CAV}

E_{SURF}

(b)

$\uparrow H^+$

$\log i$

E_{CAV}

E_{SURF}

(c)

COMBINATIONS

E, Cl^-

$\log i$

ϕ

E_{SURF}

$E_{CAV(x,t)}$

(d)

E, H^+

$\log i$

ϕ

E_{SURF}

$E_{CAV(x,t)}$

(e)

PASSIVE LAYER

$E_{A/P}$

E_{LIM}

a

$x = 0$

x

13

Hydrogen Evolution Reaction

b

a

$H_2(g)$

$x = 0$

x

$x + dx$

H^+Y^-

$x = L$

3

LARGE BUBBLE

NO BUBBLE

CALCULATED

POTENTIAL ϕ, V

DISTANCE INTO SLOT x, cm

14

20μm

FIG 15

FIG. 16

16

CONCENTRATION $[H^+] = [Y^-]$, mol L^{-1}

DISTANCE INTO SLOT X, cm

$a = 0.5$ cm

0.05

0.005

17

$$E_{LIM} = E_{M/M^{z+}}^{eq}$$

(a)

ANODIC CURRENT

$x = L$ $x = 0$

$M \rightarrow M^{z+} + ze^-$

ϕ

$E_{M/M^{z+}}^{eq}$ $E_{x=L}$ $E_{x=0}$

$$E_{LIM} = E_{H/H^+}^{eq}$$

(b)

CATHODIC CURRENT

$x = 0$ $x = L$

$H^+ + e^- \rightarrow 1/2\, H_2$

ϕ

$E_{x=0}$ $E_{x=L}$

ELECTRODE POTENTIAL $\rightarrow$ (+)

15

(a)

(b)

ELECTRODE POTENTIAL ⟶ (+)

19

CONCENTRATION $[H^+] = [ClO_4^-]$

DISTANCE

FIG. 21 PICKERING
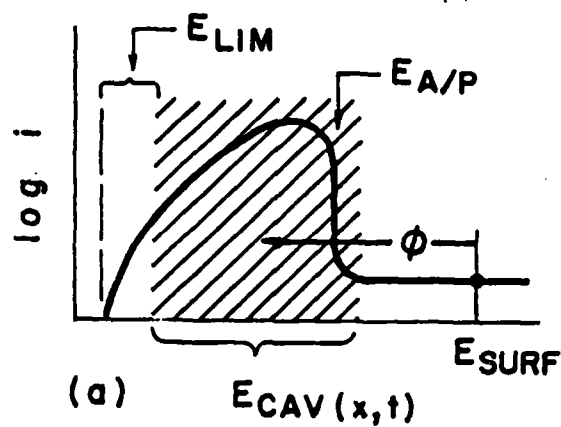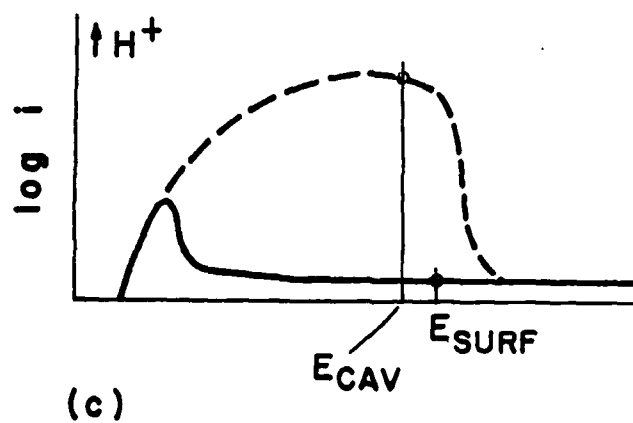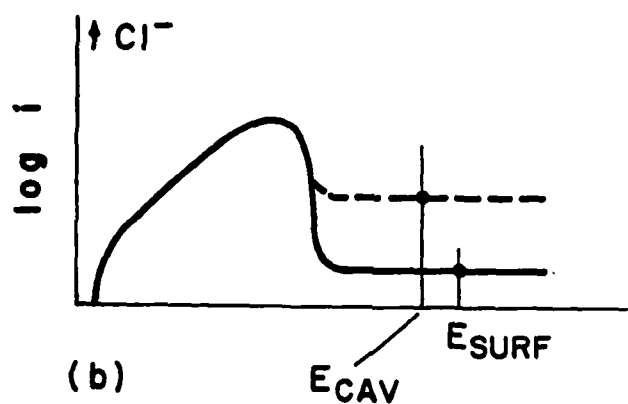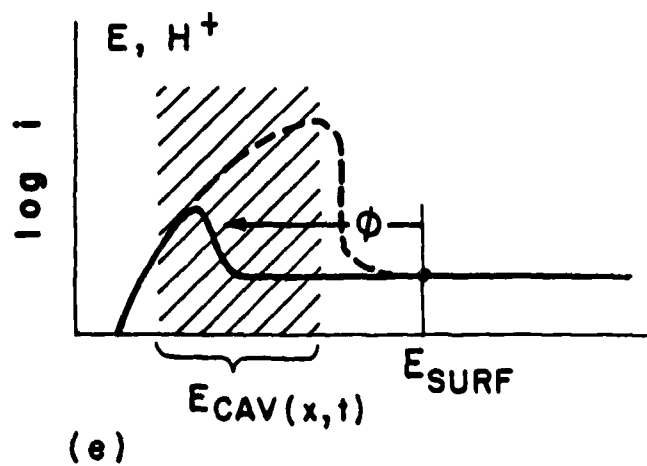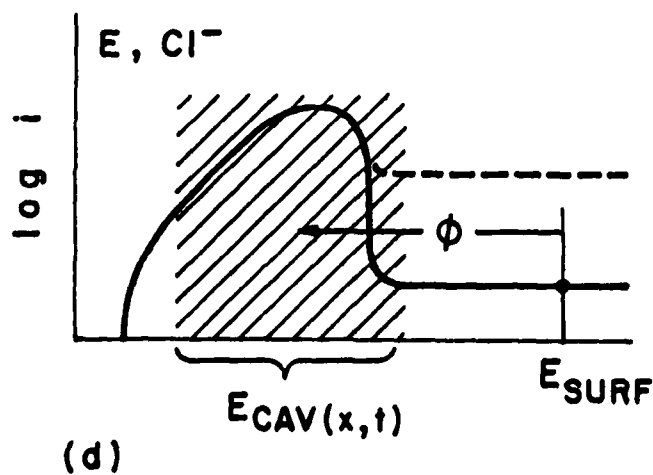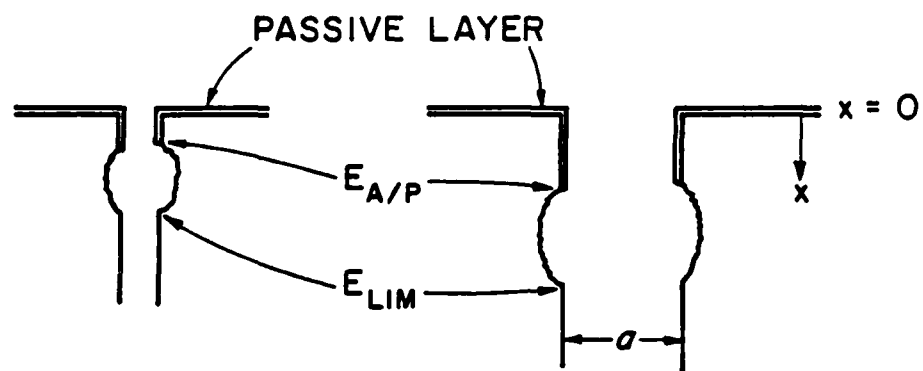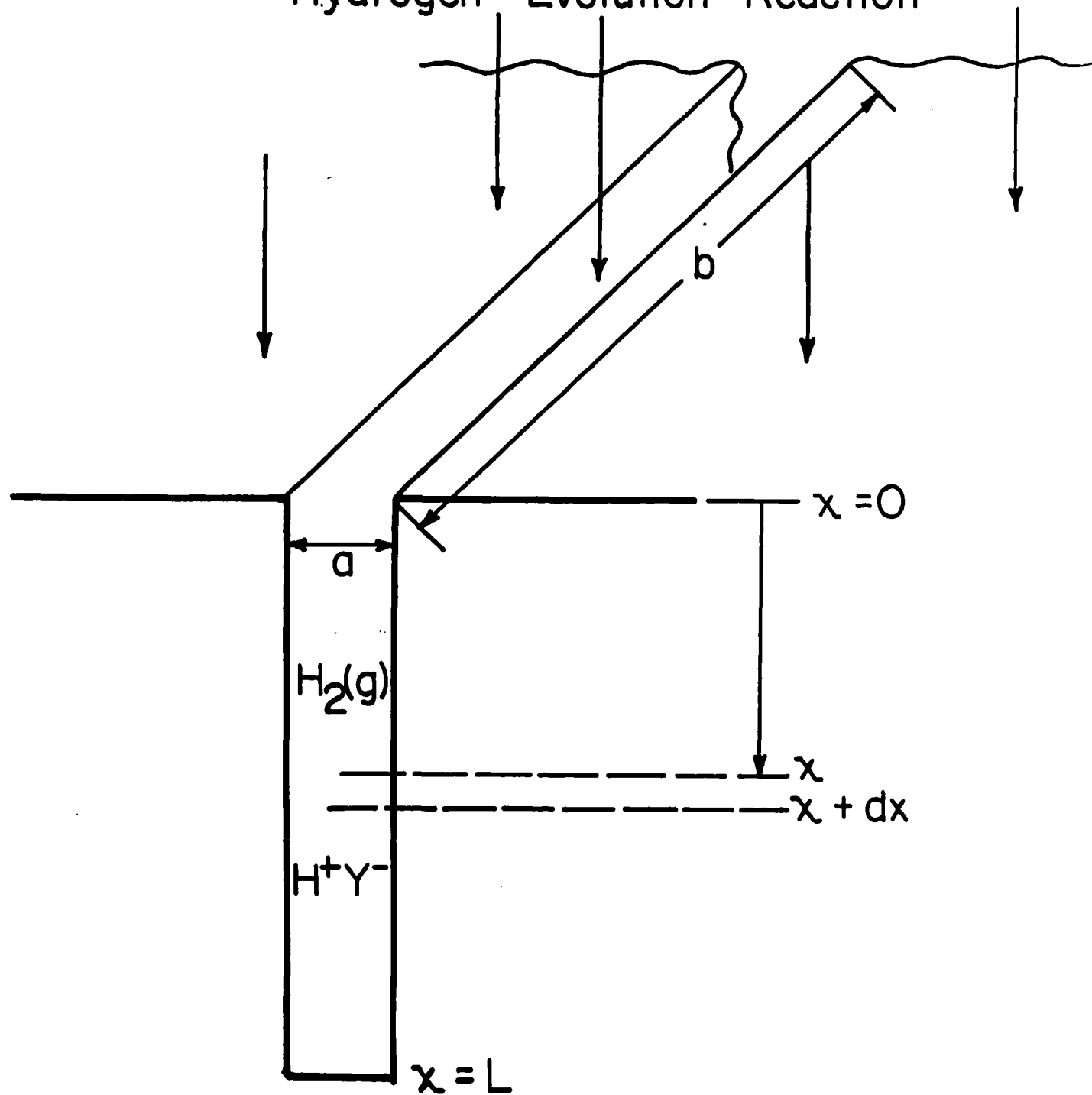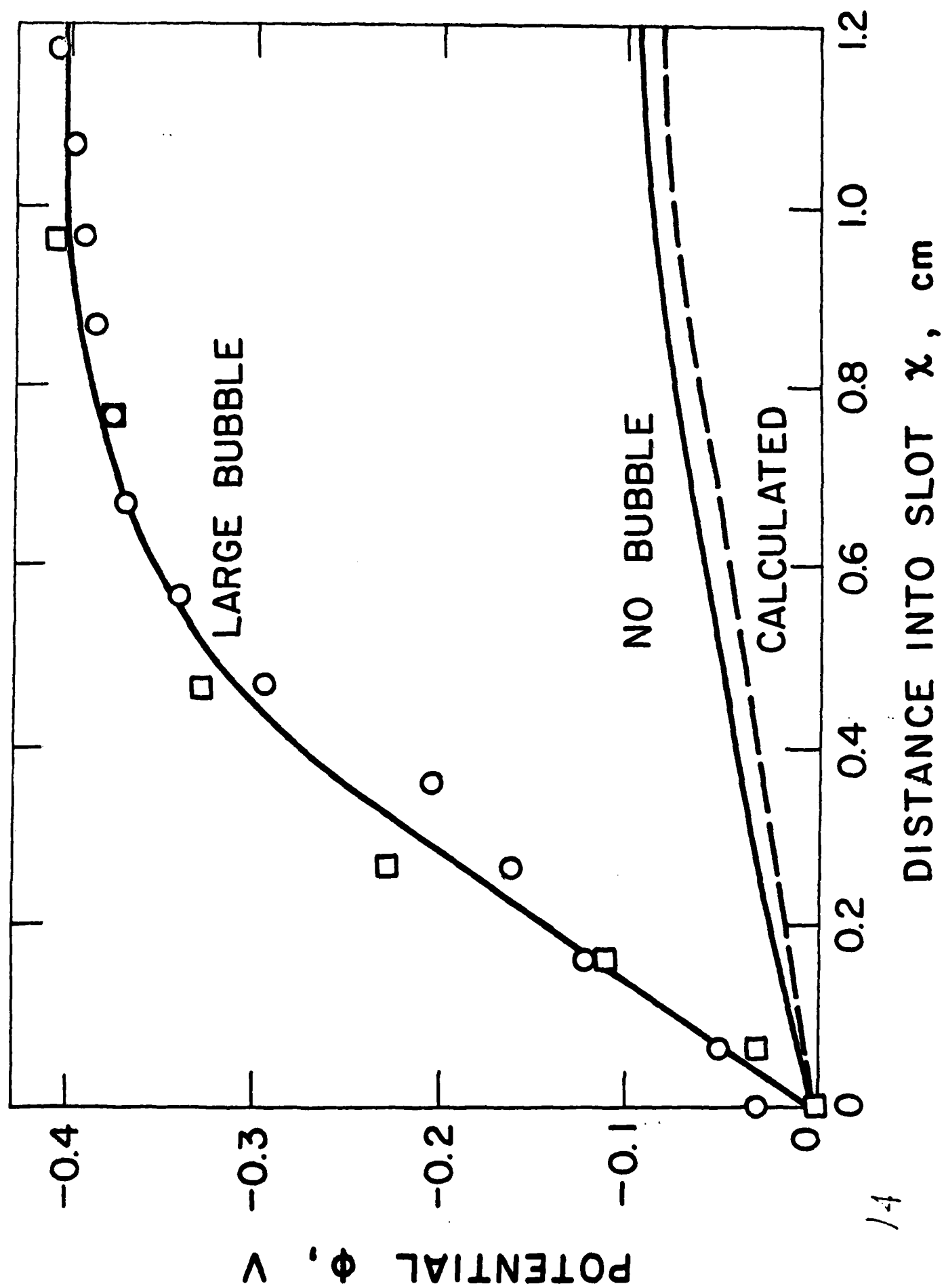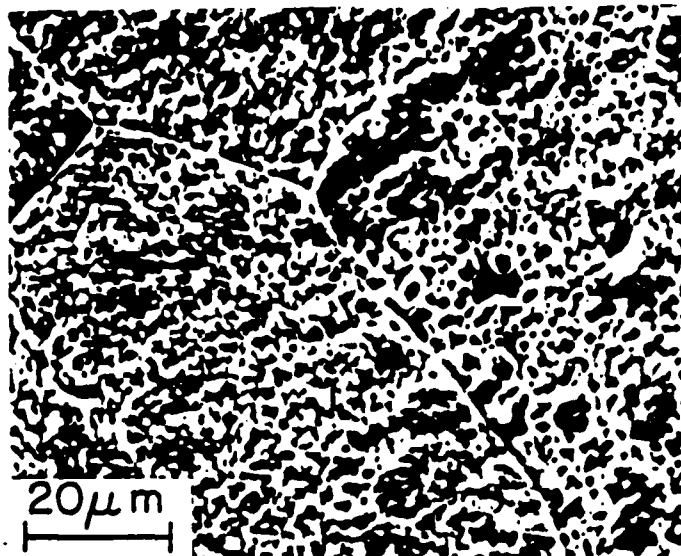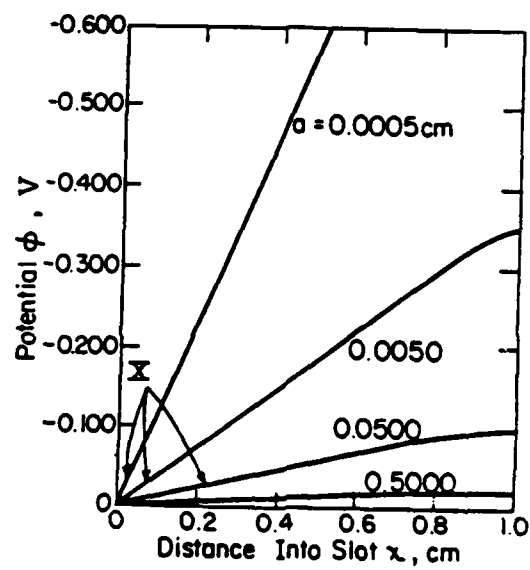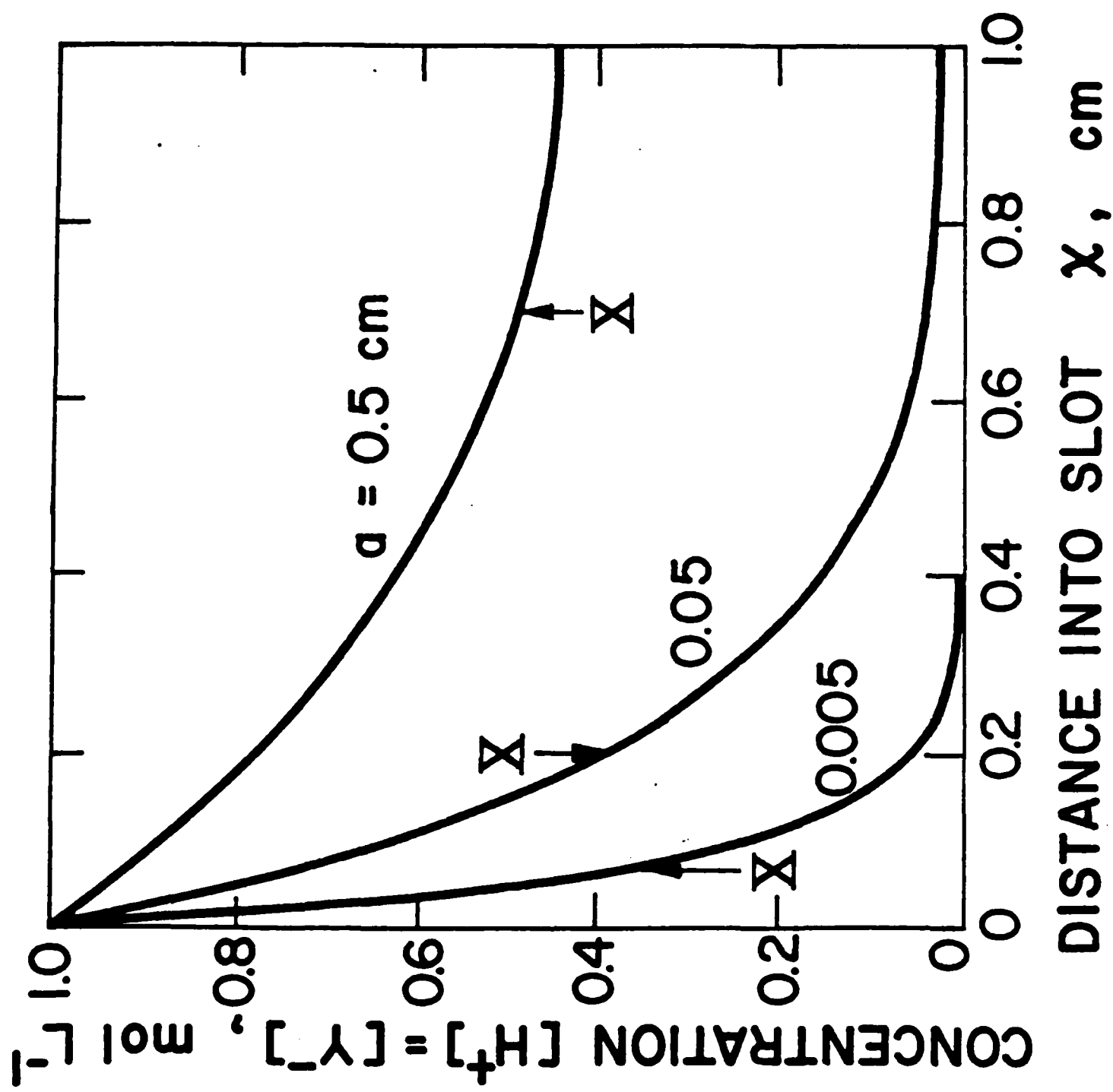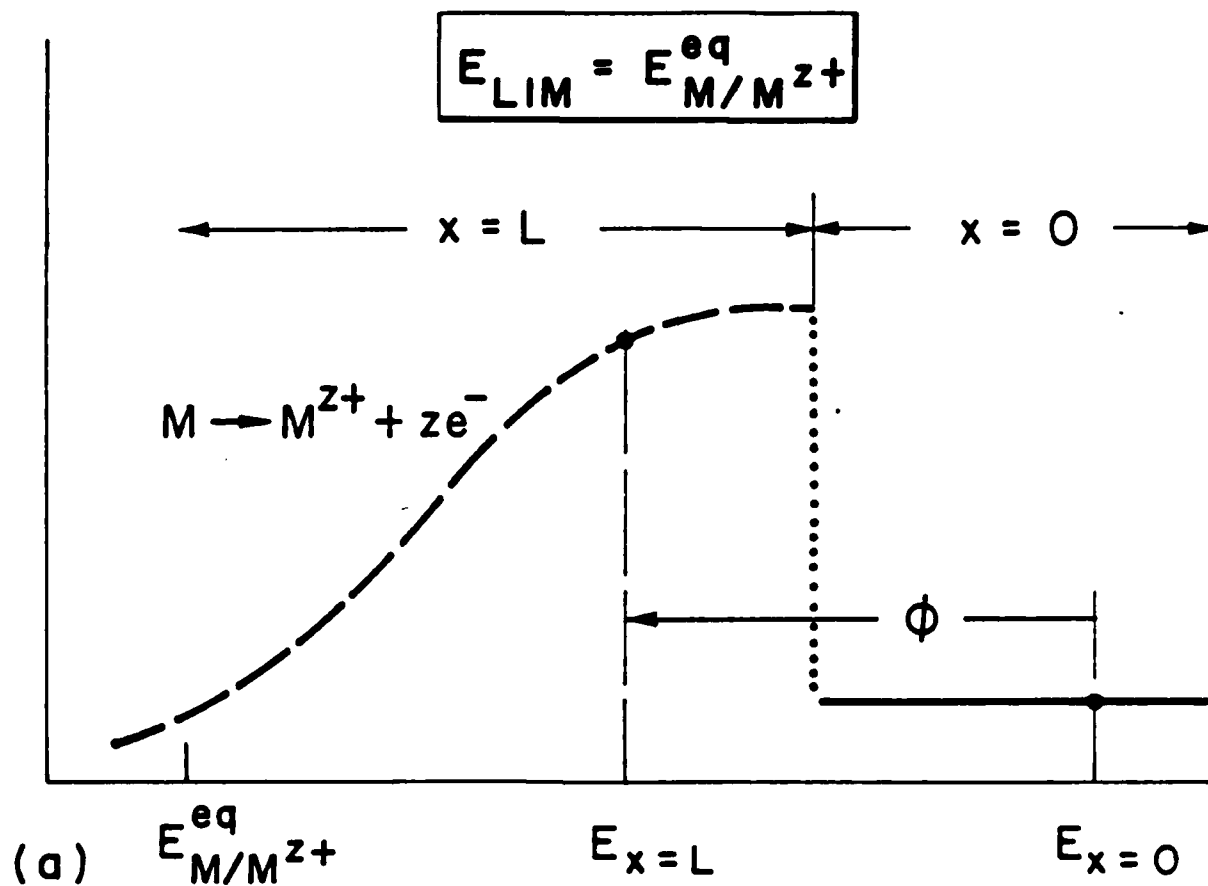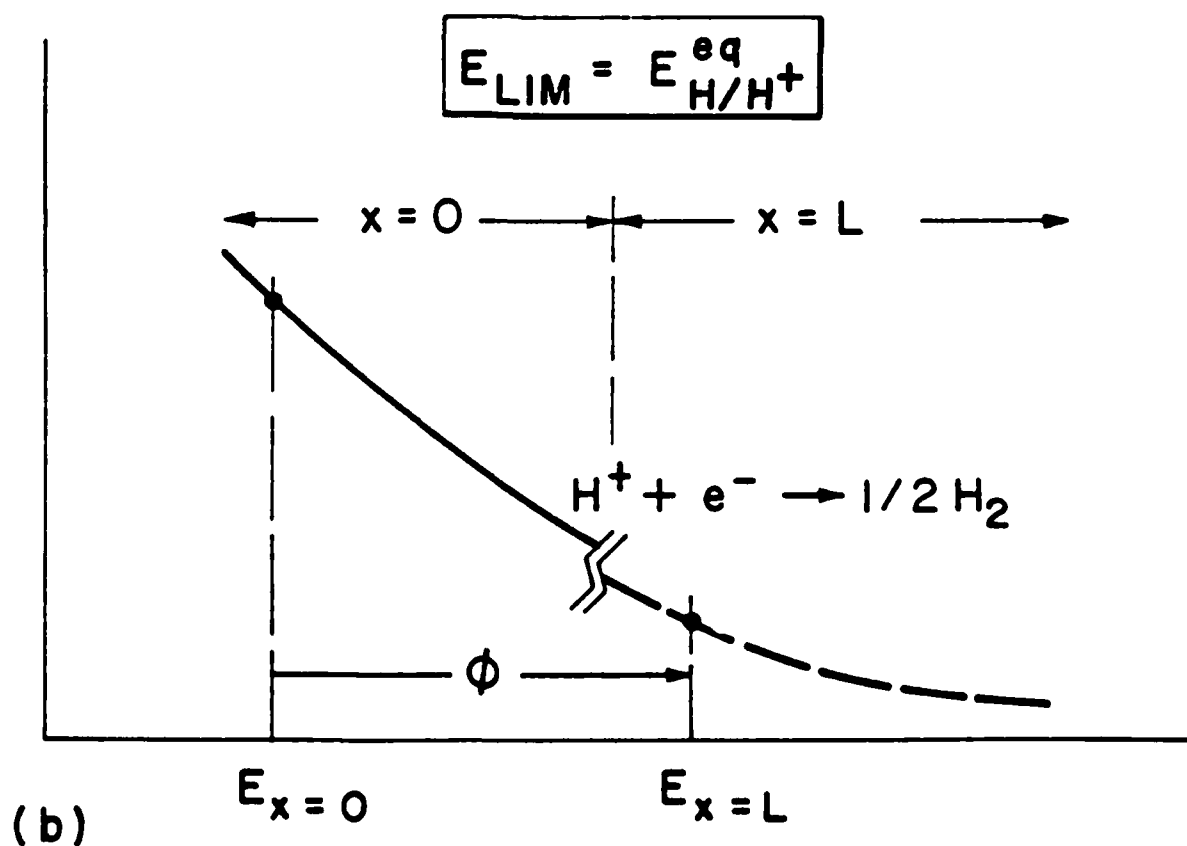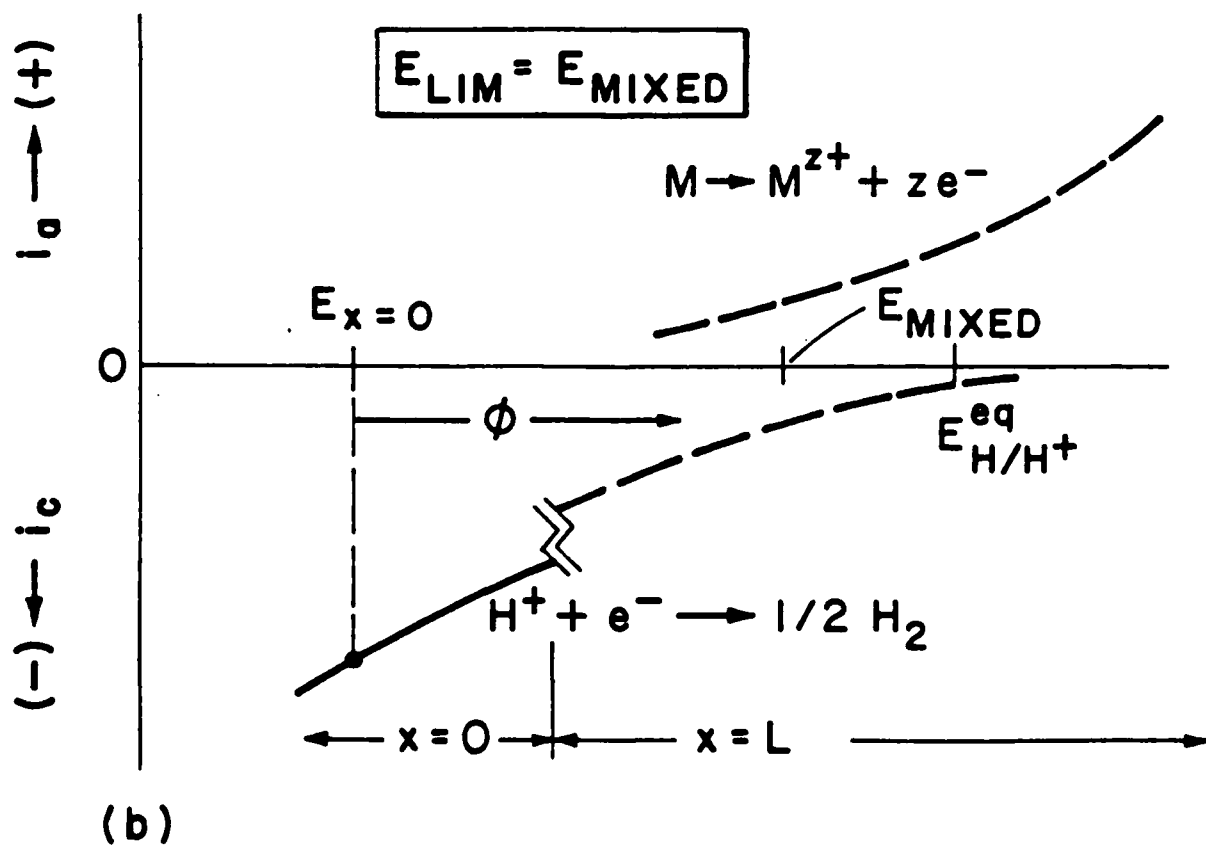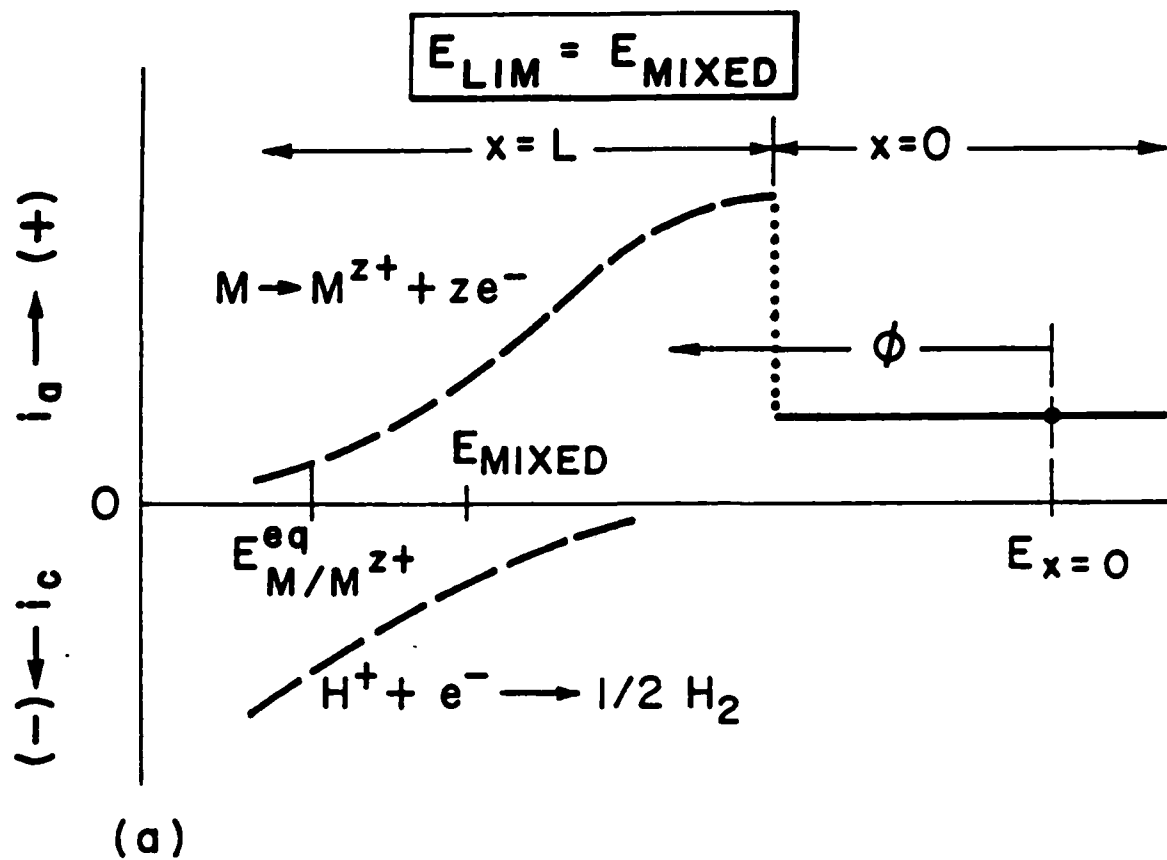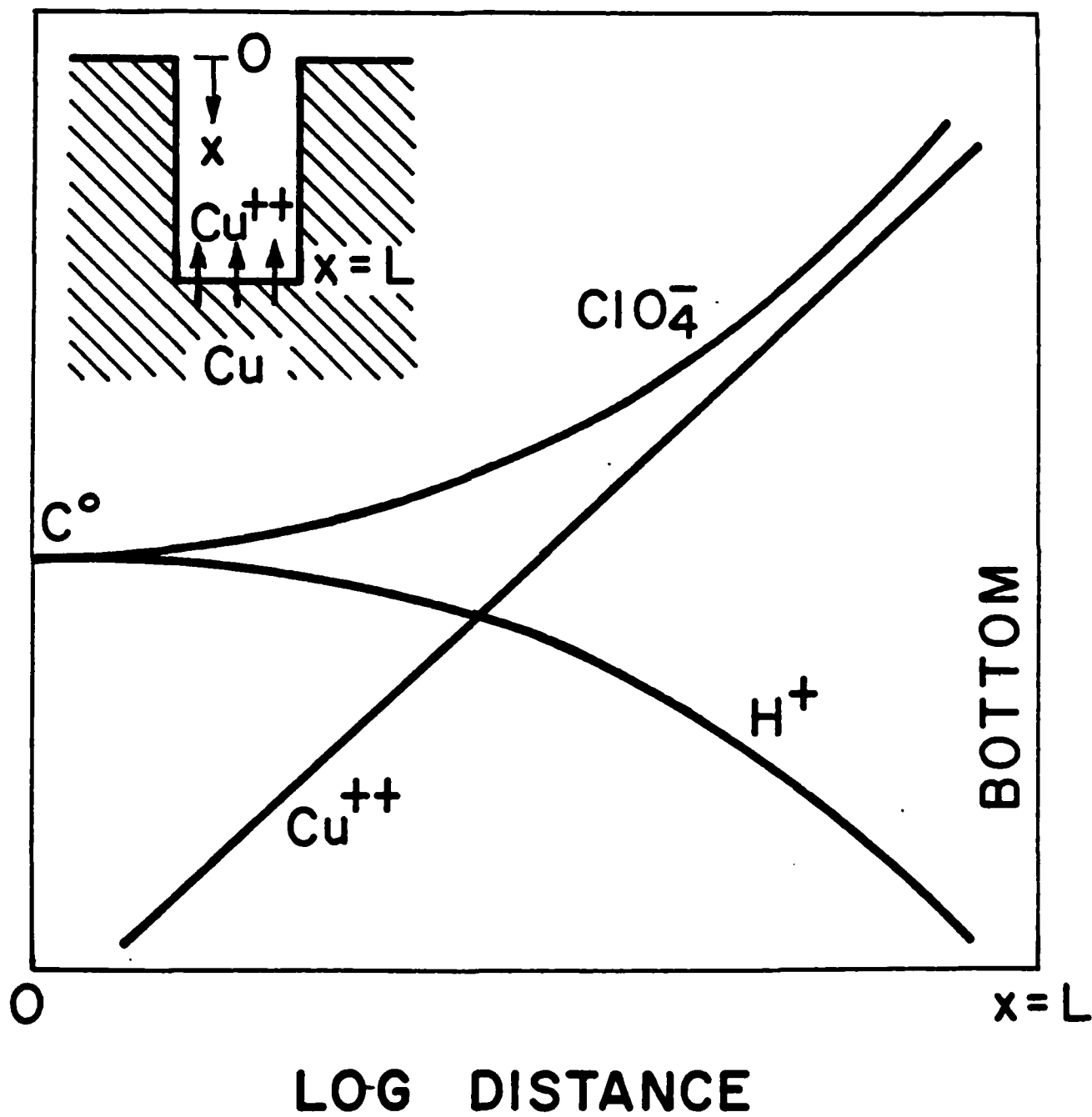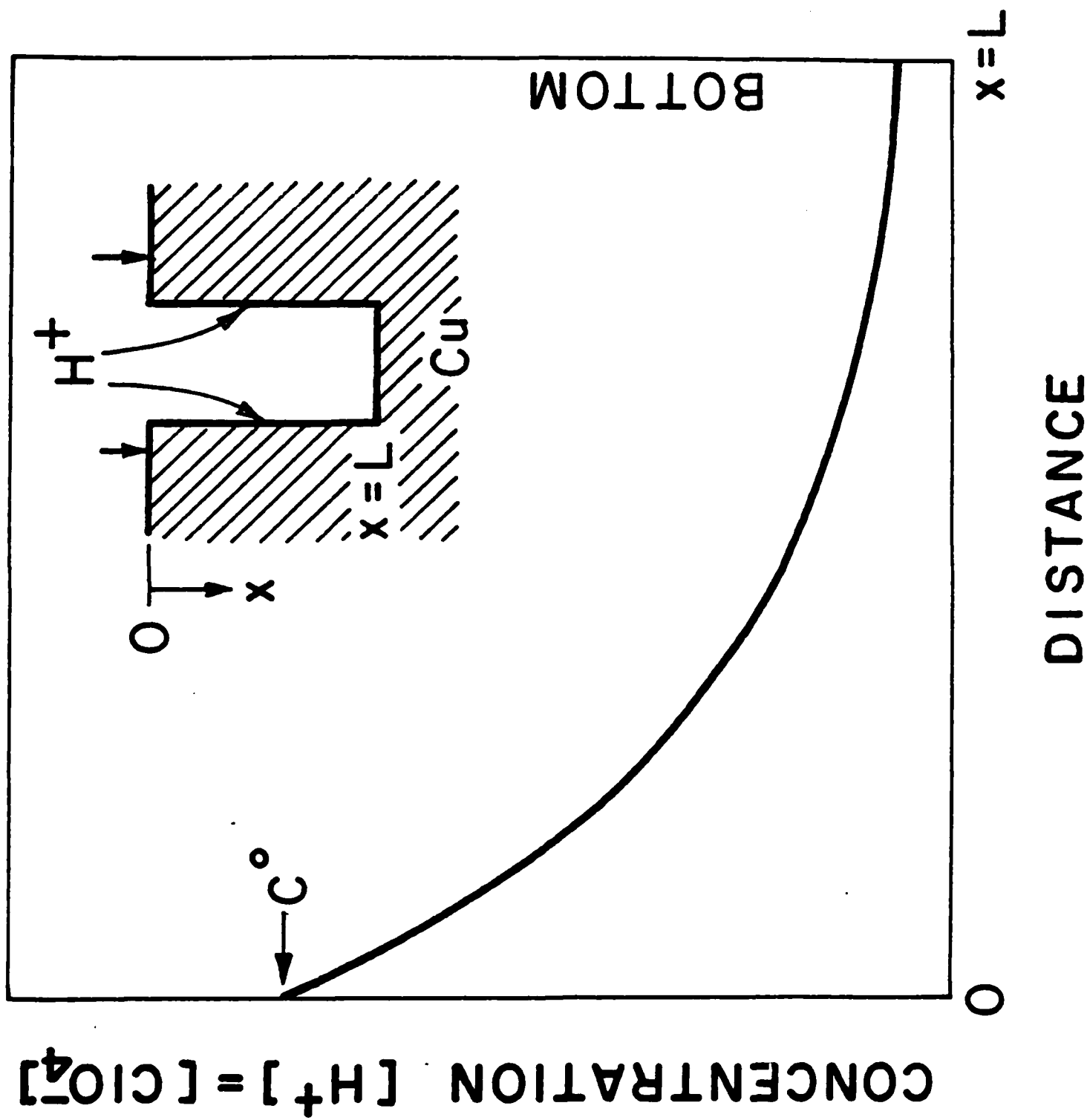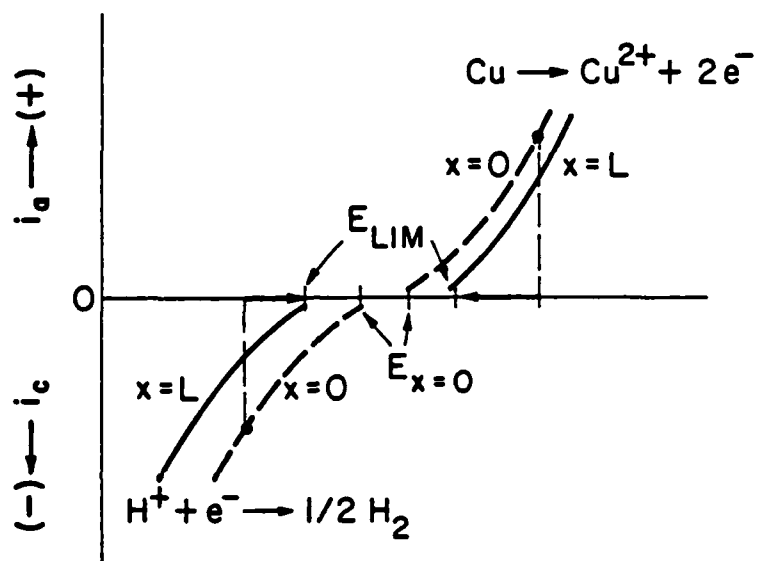
Supplemental Distribution List   Jan 1985

Prof. I.M. Bernstein
Dept. of Metallurgy and Materials Science
Carnegie-Mellon University
Pittsburgh, PA 15213

Profs. G.H. Meier and F.S. Pettit
Dept. of Metallurgical and
Materials Eng.
University of Pittsburgh
Pittsburgh, PA 15261

Prof. H.K. Birnbaum
Dept. of Metallurgy & Mining Eng.
University of Illinois
Urbana, Ill 61801

Dr. J.R. Pickens
Martin Marietta Laboratories
1450 South Rolling Rd.
Baltimore, MD 21227-3898

Dr. D.H. Boone
Department of Mechanical Eng.
Naval Postgraduate School
Monterey, Ca 93943

Prof. H.W. Pickering
Dept. of Materials Science and
Eng.
The Pennsylvania State
University
University Park, PA 16802

Dr. C.R. Crowe
Code 6372
Naval Research Laboratory
Washington, D.C. 20375

Prof. R. Summit
Dept. of Metallurgy Mechanics
and Materials Science
Michigan State University
East lansing, MI 48824

Prof. D.J. Duquette
Dept. of Metallurgical Eng.
Rensselaer Polytechnic Inst.
Troy, NY 12181

Prof. R.P. Wei
Dept. of Mechanical Engineering
and Mechanics
Lehigh University
Bethlehem, PA 18015

Prof. J. P. Hirth
Dept. of Metallurgical Eng
The Ohio State University
Columbus, OH 43210

Prof. A.J. Ardell
Dept. of Materials Science and Eng.
School of Engineering & Applied
Scinece
University of California at
Los Angleles
Los Angeles, CA 90024

Dr. R.G. Kasper
Code 4493
Naval Underwater Systems Center
New London, CT 06320

Prof. B.E. Wilde
Fontana Corrosion Center
Dept. of Metallurgical Eng.
The Ohio State University
116 west 19th Ave.
Columbus, OH 43210

Prof. H. Leidheiser, Jr.
Center for coatings and Surface Research
Sinclair Laboratory, Bld. No. 7
Lehigh University
Bethlehem, PA 18015

Dr. C. R. Clayton
Department of Materials Science
& Engineering
State University of new York
Stony Brook
Long Island, New York 11794

Dr. F. Mansfeld
Rockwell International - Science Center
1049 Camino Dos Rios
P.O. Box 1085
Thousand Oaks, CA 91360

BASIC DISTRIBUTION LIST

Technical and Summary Reports   1985

Organization	Code	Organization	Copies
Defense Documentation Center Cameron Station Alexandria, VA 22314	12	Naval Air Propulsion Test Center Trenton, NJ 08628 ATTN: Library	1
Office of Naval Research Department of the Navy 800 N. Quincy Street Arlington, VA 22217 Attn: Codes 431	3	Naval Electronics Laboratory San Diego, CA 92152 ATTN: Electron Materials Sciences Division	1
Naval Research Laboratory Washington, DC 20375 ATTN: Codes 6000 6300 2627	1 1 1	Naval Missile Center Materials Consultant Code 3312-1 Point Mugu, CA 92041	1
Naval Air Development Center Code 606 Warminster, PA 18974 ATTN: Dr. J. DELuccia	1	Naval Construction Battallion Civil Engineering Laboratory Port Hueneme, CA 93043 ATTN: Materials division	1
Commanding Officer Naval Surface Weapons Center White Oak Laboratory Silver Spring, MD 20910 ATTN: Library	1	Commander David W. Taylor Naval Ship Research and Development Center Bethesda, MD 20084	1
Naval Oceans Systems Center San Diego, CA 92132 ATTN: Library	1	Naval Underwater System Center Newport, RI 02840 ATTN: Libary	1
Naval Postgraduate School Monterey, CA 93940 ATTN: Mechanical Engineering Department	1	Naval Weapons Center China Lake, CA 93555 ATTN: Library	1
Naval Air Systems Command Washington, DC 20360 ATTN: Code 310A Code 5304B	1 1	NASA Lewis Research Center 21000 Brookpark Road Cleveland, OH 44135 ATTN: Library	1
Naval Sea System Command Washington, DC 20362 ATTN: Code 05R	1	National Bureau of Standards Washington, DC 20234 ATTN: Metals Science and Stands Division Ceramics Glass and Solid State Science Division Fracture and Deformation Div.	1 1 1

Naval Facilities Engineering
  Command
Alexandria, VA 22331
ATTN: Code 03   1

Scientific Advisor
Commandant of the Marine Corps
Washington, DC 20380
ATTN: Code AX   1

Army Research Office
P. O. Box 12211
Triangle Park, NC 27709
ATTN: Metallurgy & Ceramics
       Program   K   1

Army Materials and Mechanics
  Research Center
Watertown, MA 02172
ATTN: Research Programs
       Office   1

Air Force Office of Scientific
   Research/NE
Building 410
Bolling Air foce Base
Washington, DC 20332
ATTN: Electronics & Materials
       Science Directorate   1

NASA Headquarters
Washington, DC 20546
ATTN: Code RRM   1

Mr. Michael T. McCracken
Office of Naval Research Resident
 Representative
National Academy of Sciences,
  Joseph Henry Bldg.,
Room 623, 2100 Pennsylvania Avenue,
  N.W.
Washington, D.C. 20037   1

Defense Metals and Ceramics
  Information Center
Battelle Memorial Institute
505 King Avenue
Columbus, Oh 43201   1

Metals and Ceramics Division
Oak Ridge National Laboratory
P.O. Box X
Oak Ridge, TN 37380   1

Los Alamos Scientific Laboratory
P.O. Box 1663
Los Alamos, NM 87544
ATTN: Report Librarian   1

Argonne National Laboratory
Metallurgy Division
P.O. Box 229
Lemont, IL 60439   1

Brookhaven National Laboratory
Technical Information Division
Upton, Long Island
New York 11973
ATTN: REsearch Library   1

Library
Building 50 Room 134
Lawrence Radiation Laboratory
Berkeley, CA   1

END

FILMED

2 4-86

DTIC